C2 Continuous Blending of Time-Dependent Parametric Surfaces

Xiangyu You[1]
Faculty of Science and Technology, Bournemouth University, Talbot Campus, Poole, BH12 5BB, United Kingdom

Feng Tian
Faculty of Science and Technology, Bournemouth University, Talbot Campus, Poole, BH12 5BB, United Kingdom

Wen Tang
Faculty of Science and Technology, Bournemouth University, Talbot Campus, Poole, BH12 5BB, United Kingdom

ABSTRACT

Surface blending is frequently met in mechanical engineering. Creating a smooth transition surface of C^2 continuity between time-dependent parametric surfaces that change their positions and shapes with time is an important and unsolved topic in surface blending. In order to address this issue, this paper develops a new approach to unify both time-dependent and time-independent surface blending with C^2 continuity. It proposes a new surface blending mathematical model consisting of a vector-valued sixth-order partial differential equation and blending boundary constraints, and investigates a simple and efficient approximate analytical solution of the mathematical model. A number of examples are presented to demonstrate the effectiveness and applications. The proposed approach has the advantages of: (1) unifying time-independent and time-dependent surface blending, (2) always maintaining C^2 continuity at trimlines when parametric surfaces change their positions and shapes with time, (3) providing effective shape control handles to achieve the expected shapes of blending surfaces but still exactly satisfy the given

[1] Corresponding author.

blending boundary constraints, and (4) quickly generating C^2 continuous blending surfaces from the approximate analytical solution with easiness, good accuracy, and high efficiency.

Keywords: Surface blending, time-dependent and time-independent parametric surfaces, C^2 continuity, sixth-order partial differential equations, approximate analytical solutions

1 INTRODUCTION

Surface blending has many applications in mechanical engineering. It is widely applied in computer-aided design, and used to emulate manufacturing procedures, alleviate stress concentrations, or avoid flow disturbances.

Surface blending can be divided into different types. The main types of blends met in practice can be categorized as: surfaces governed by strong functional constraints, esthetic blends, fairings, and rounds and fillets [1].

Surface blending is to generate a smooth transition between intersecting surfaces or a smooth connection between disjoint surfaces. The surfaces to be blended are called primary surfaces. The surface which forms a smooth transition or connection between primary surfaces is called a blending surface. The interface curves between a blending surface and primary surfaces are called trimlines [2].

Implicit [3] and parametric [4] surfaces are two types of surface representations commonly used in modeling systems. Parametric surfaces such as NURBS surfaces are especially applicable to computer-aided design. This paper investigates blending between parametric surfaces.

Tangent and curvature continuities are most frequently applied in mechanical engineering. For example, discontinuous curvature causes problems in NC milling and leads to break points of reflection lines [5] which are widely used in automotive industry [6]. A cam with second-order discontinuity creates abrupt changes in acceleration, and the design of streamlined surfaces of aircraft, ship, and submarine requires curvature continuity to avoid flow separation and turbulence [7]. Although G^2 continuous surfaces can meet curvature continuity requirement, higher-order continuity such as continuous slope-of-curvature can suppress both laminar and turbulent separation and lead to higher aerodynamic efficiency [8]. It is also stated that higher-order (> C^2 continuous) surfaces are often required for certain numerical simulations and to meet visual, aesthetic, and functional requirements [8]. Due to the importance of C^2 continuities, this paper will investigate this issue.

Depending on whether primary surfaces change their positions and shapes with time, surface blending can be divided into time-independent and time-dependent. A comprehensive literature survey on blending time-independent parametric surfaces has been made in [2]. Although various blending methods have been developed, all these methods can only deal with time-independent primary surfaces which do not change their positions and shapes over time. However, in many situations, primary surfaces are constantly in motion and change shapes. It has been pointed out that the blending surface joining the wing of an aircraft to the fuselage must meet stringent aerodynamic requirements [1]. The blending surfaces connecting the torso and limbs of a running person must be always smooth and seamless. In spite of the importance of time-

dependent surface blending, it has not attracted a lot of research attention except for [9] which investigated time-dependent C^1 continuous surface blending. This paper will develop a new method to extend time-dependent C^1 continuity to time-dependent C^2 continuity.

Another important problem is how to achieve satisfactory shapes of blending surfaces but still maintain exact satisfaction of blending boundary constraints. Kiciak [10] introduced a function which is the integral of the square of length of the mean curvature gradient with respect to the surface measure and minimized the functional to achieve a satisfactory shape of a blending surface. The numerical minimization algorithm involves heavy computations. Unlike the minimization algorithm, the approach proposed in this paper directly adjusts the values of shape control parameters to achieve a satisfactory shape of blending surfaces easily and quickly.

To summarize, the main contributions of this paper are: (1) a new approach to generate time-dependent blending surfaces and unify both time-dependent and time-independent surface blending with C^2 continuity, (2) a new C^2 continuous and time-dependent surface blending mathematical model and its simple and efficient approximate analytical solution, and (3) powerful shape control handles to achieve a satisfactory shape of blending surfaces.

The rest of this paper is organized as follows. The related work is briefly reviewed in Section 2. The mathematical model of time-dependent surface blending with C^2 continuity is formulated in Section 3. A simple and efficient approximate analytical solution of the mathematical model is developed in Section 4. The accuracy,

efficiency, and effects of second partial derivatives and shape control parameters of the proposed approximate analytical solution are investigated in Section 5. The applications of the proposed approach in time-dependent and time-independent surface blending are demonstrated in Section 6, and the conclusion and future work are discussed in Section 7.

2 RELATED WORK

Various time-independent methods have been proposed to blend parametric surfaces. Among them, rolling ball methods, which can be divided into constant radius [11] and variable radius [12] ones, are most widely used for rounding edges and corners of mechanical parts [13]. In addition, the potential method [14-16] was also proposed.

The shapes of the blending surfaces created by rolling-ball methods are circular. Noncircular blending surfaces can be generated with some other methods such as filling n-sided regions [17], polyhedral vertex blending with setbacks using rational S-patches [18], branching blends between two natural quadrics with Pythagorean normal surfaces [19], and partial differential equation (PDE)-based methods [20].

PDE-based methods are most powerful in creating different noncircular shapes of blending surfaces. They formulate surface blending as a mathematical boundary-value problem, and adjust shape control parameters embedded in the PDE to effectively generate different shapes of blending surfaces while still keeping exact satisfaction of blending boundary constraints.

The earliest work about PDE-based surface blending was described in [20]. How to solve partial differential equations effectively and efficiently is a most important issue. Numerical, accurate, and approximate analytical methods can be used to solve partial differential equations. Various numerical methods such as the finite difference method [21] and the finite element method [22] are most powerful. In spite of their powerful capacity, they have the following limitations. First, they generate blending surfaces with discrete boundary representations which are unsuitable for the requirement of good continuity. Second, they involve many design variables and a lot of calculations which cause high requirements for computing devices and slow response. Third, specific knowledge and skills of the numerical methods are required to carry out the numerical calculations.

In contrast, accurate and approximate analytical methods can overcome these limitations with less powerful capacity. Accurate methods obtain the closed form solution of partial differential equations, but only apply to some simple and special cases [23]. Approximate analytical methods [24] are more powerful than accurate methods and more efficient but more difficult to obtain than numerical methods. In this paper, we have adopted approximate analytical methods to develop a new surface blending approach.

Up to now, most PDE-based methods and all other surface blending approaches only investigate time-independent surface blending. The work described in [9] initiated the research on surface blending of time-dependent parametric surfaces. It proposed a vector-valued fourth-order partial differential equation involving a time variable and the

constraints of positional and tangential (first partial derivative) continuities and its approximate analytical solution to generate time-dependent surface blending of C^1 continuity. The method is not applicable to time-independent surface blending since the solution of the partial differential equation always involves the time variable. In addition, C^2 continuous surface blending has not been investigated.

In order to tackle the above problems and generalize the technique introduced in [9], this paper drops the time variable, proposes sixth-order partial differential equations, introduces the second partial derivative continuity into blending boundary constraints to address C^2 continuity, and develops the first approximate analytical solution of the sixth-order partial differential equations to unify both time-independent and time-dependent C^2 continuous surface blending. It has the advantages of easiness, good accuracy, and high efficiency.

3 MATHEMATICAL MODEL OF SURFACE BLENDING WITH C^2 CONTINUITY

The mathematical model of PDE-based surface blending consists of partial differential equations for x, y and z components and blending boundary constraints. When two primary parametric surfaces are to be connected together with C^2 continuity, the blending surface must satisfy the constraints of the position functions and the first and second partial derivatives of the two primary parametric surfaces at the trimlines. If the two primary parametric surfaces change their shape with the time, the position functions and the first and second partial derivatives of the primary parametric surfaces at the trimlines are the functions of time variable t. Therefore, the

two primary parametric surfaces can be written as $\mathbf{S}_1(u,v,t)$ and $\mathbf{S}_2(u,v,t)$ where u and v are the parametric variables and t is a time variable, and the position function and the first and second partial derivatives for the first primary parametric surface $\mathbf{S}_1(u,v,t)$ at the trimline $u=u_0$ can be written as $\mathbf{C}_1(v,t)$, $\mathbf{C}_2(v,t)$ and $\mathbf{C}_3(v,t)$, and those for the second primary parametric surface $\mathbf{S}_2(u,v,t)$ at the trimline $u=u_1$ can be written as $\mathbf{C}_4(v,t)$, $\mathbf{C}_5(v,t)$ and $\mathbf{C}_6(v,t)$ where u_0 and u_1 are two specified values between 0 and 1.

Assuming the mathematical equation of the blending surface is $\mathbf{S}(u,v,t)$, its position function, and the first and second partial derivatives at the trimlines $u=0$ and $u=1$ must be the same as those of the primary parametric surfaces at the trimlines. Therefore, the boundary constraints of the blending surface between the two primary parametric surfaces can be written as

$$\begin{aligned} &u=0 \quad \partial^n\mathbf{S}(u,v,t)/\partial u^n=\mathbf{C}_{n+1}(v,t)\\ &u=1 \quad \partial^n\mathbf{S}(u,v,t)/\partial u^n=\mathbf{C}_{n+4}(v,t)\\ &(n=0,1,2) \end{aligned} \tag{1}$$

where $\partial^0\mathbf{S}(u,v,t)/\partial u^0=\mathbf{S}(u,v,t)$, $\mathbf{S}(u,v,t)$ has three components $S_x(u,v,t)$, $S_y(u,v,t)$, and $S_z(u,v,t)$, and $\mathbf{C}_i(v,t)$ $(i=1,2,\cdots,6)$ also have three components $C_{xi}(v,t)$, $C_{yi}(v,t)$, and $C_{zi}(v,t)$.

Equation (1) is a general form of blending boundary constraints. Here we give an example to demonstrate how to determine its concrete form. This example is to smoothly connect two primary parametric surfaces together. The parametric representation for the first primary surface is

$$x = aue^{t}\sin 2\pi v \qquad y = bue^{-t}\cos 2\pi v \qquad z = h_1 + h_2 u^2 \tag{2}$$

and the parametric representation for the second primary surface is

$$x = cue^{-t}\sin 2\pi v \qquad y = due^{t}\cos 2\pi v \qquad z = -h_3 u^3 \tag{3}$$

where a, b, c, d, h_1, h_2 and h_3 are the geometric parameters to be specified, and $0 \le u \le 1.$

Setting the geometric parameters in Eq. (2) and (3) to be: $a = 3.6$, $b = 5.5$, $c = 6.0$, $d = 3.0$, $h_1 = 2.0$, $h_2 = 6.0$, and $h_3 = 20.0$, the first primary surface between $u = 0.4$ and $u = 0.75$ and the second primary surface between $u = 0.55$ and $u = 0.65$ at the time instants $t = 0$, 0.2, 0.4, 0.6, 0.8, and 1.0 are depicted in Fig. 1 where the top and bottom primary surfaces are obtained from Eq. (2) and Eq. (3), respectively.

If we take the trimline to be $u = u_0$ in Eq. (2) for the top primary surface and $u = u_1$ in Eq. (3) for the bottom primary surface, we obtain the boundary curves $\mathbf{C}_1(v,t) = \left[au_0 e^{t}\sin 2\pi v \quad bu_0 e^{-t}\cos 2\pi v \quad h_1 + h_2 u_0^2\right]^T$ and $\mathbf{C}_4(v,t) = \left[cu_1 e^{-t}\sin 2\pi v \quad du_1 e^{t}\cos 2\pi v \quad -h_3 u_1^3\right]^T$. With Eqs. (2) and (3), we can derive the first partial derivatives $\partial x/\partial u$, $\partial y/\partial u$, and $\partial z/\partial u$, and the second partial derivatives $\partial^2 x/\partial u^2$, $\partial y^2/\partial u^2$, and $\partial^2 z/\partial u^2$. Setting $u = u_0$ for the partial derivatives from Eq. (2), we obtain $\mathbf{C}_2(v,t) = \left[-ae^{t}\sin 2\pi v \quad -be^{-t}\cos 2\pi v \quad -2h_2 u_0\right]^T$ and $\mathbf{C}_3(v,t) = \left[0 \quad 0 \quad 2h_2\right]^T$. Setting $u = u_1$ for the partial derivatives from Eq. (3), we obtain $\mathbf{C}_5(v,t) = \left[ce^{-t}\sin 2\pi v \quad de^{t}\cos 2\pi v \quad -3h_3 u_1^2\right]^T$ and $\mathbf{C}_6(v,t) = \left[0 \quad 0 \quad -6h_3 u_1\right]^T$. Substituting $\mathbf{C}_i(v,t)$ $(i = 1,2,\cdots,6)$ into (1), boundary constraints (1) become

$$
\begin{array}{lll}
u=0 & S_x = au_0 e^{t}\sin 2\pi v & S_y = bu_0 e^{-t}\cos 2\pi v \qquad S_z = h_1 + h_2 u_0^2 \\
 & \dfrac{\partial S_x}{\partial u} = -ae^{t}\sin 2\pi v & \dfrac{\partial S_y}{\partial u} = -be^{-t}\cos 2\pi v \qquad \dfrac{\partial S_z}{\partial u} = -2h_2 u_0 \\
 & \dfrac{\partial^2 S_x}{\partial u^2} = 0 & \dfrac{\partial^2 S_y}{\partial u^2} = 0 \qquad \dfrac{\partial^2 S_z}{\partial u^2} = 2h_2 \\
u=1 & S_x = cu_1 e^{-t}\sin 2\pi v & S_y = du_1 e^{t}\cos 2\pi v \qquad S_z = -h_3 u_1^3 \\
 & \dfrac{\partial S_x}{\partial u} = ce^{-t}\sin 2\pi v & \dfrac{\partial S_y}{\partial u} = de^{t}\cos 2\pi v \qquad \dfrac{\partial S_z}{\partial u} = -3h_3 u_1^2 \\
 & \dfrac{\partial^2 S_x}{\partial u^2} = 0 & \dfrac{\partial^2 S_y}{\partial u^2} = 0 \qquad \dfrac{\partial^2 S_z}{\partial u^2} = -6h_3 u_1
\end{array}
\tag{4}
$$

For C^2 continuous surface blending introduced in [9], the first and second partial derivatives of blending surfaces with respect to a time variable t are involved in a vector-valued partial differential equation. In spite of the advantage in considering the effects of acceleration and velocity, it will cause the following problem. When primary surfaces are time-independent and do not change their positions and shapes, the blending surface should also be time-independent and does not change its position and shape. However, since the first and second partial derivatives of blending surfaces with respect to the time variable t are involved in the vector-valued partial differential equation, its closed form solution involves the time variable t and the blending surface defined by the closed form solution will change its shape with time. This is contradictory to the real situation and makes the surface blending technique in [9] unsuitable for time-independent surface blending. In order to generalize the technique introduced in [9] and unify both time-dependent and time-independent surface blending, this paper will remove the two terms involving the first and second partial derivatives with respect

to the time variable t. Such a treatment also simplifies the mathematical operation and raises the computational efficiency.

For PDE-based surface blending, boundary constraints determine the order of partial differential equations necessary to achieve the required continuity. If C^2 continuity is required, the blending and primary surfaces share two position functions, two first partial derivatives, and two second partial derivatives at the trimlines $u=0$ and $u=1$ as shown in Eq. (1). The closed form solution of a vector-valued sixth-order partial differential equation contains 6 unknown constants. They can be used to satisfy the 6 constraints given in blending boundary constraints (1). Therefore, we choose the following sixth-order partial differential equations

$$(\gamma\frac{\partial^6}{\partial u^6}+\eta\frac{\partial^6}{\partial u^4\partial v^2}+\lambda\frac{\partial^6}{\partial u^2\partial v^4}+\rho\frac{\partial^6}{\partial v^6})S_\xi(u,v,t)=0 \quad (\xi=x,y,z) \tag{5}$$

subjected to the blending boundary constraints (1) for C^2 continuous surface blending. In the equation, γ, η, λ, and ρ are called shape control parameters since they have a big influence on the shapes of blending surfaces.

Putting Eq. (5) and Eq. (1) together, we obtain the mathematical model of C^2 continuous blending of time-dependent parametric surfaces. Its approximate analytical solution will be developed below.

For time-independent primary surfaces, the time variable t in the partial differential equations (5) and the blending boundary constraints (1) drops, and the

corresponding mathematical model consisting of equations (5) and (1) becomes time-independent which can be used to deal with time-independent surface blending.

4 APPROXIMATE ANALYTICAL SOLUTION OF MATHEMATICAL MODEL

It is difficult to directly solve the sixth-order partial differential equations (5) subjected to the blending boundary constraints (1). In order to simplify the solution, we examine the boundary functions $f_{\xi i}(v,t)$ $(\xi = x,y,z; i = 1,2,\cdots)$ given in the blending boundary constraints (1) and classify the boundary functions into three groups

$$\begin{aligned} &\overline{C}_{\xi n} = \overline{C}_{\xi n}(v,t) = \sum_j \overline{a}_{\xi j,n}\, \bar{f}_{\xi j}(v,t) \qquad \hat{C}_{\xi n} = \hat{C}_{\xi n}(v,t) = \sum_k \hat{a}_{\xi k,n}\, \hat{f}_{\xi k}(v,t) \\ &\widetilde{C}_{\xi n} = \widetilde{C}_{\xi n}(v,t) = \sum_l \widetilde{a}_{\xi l,n}\, \widetilde{f}_{\xi l}(v,t) \\ &(j,k,l = 1,2,\cdots; n = 1,2,\cdots,6) \end{aligned} \tag{6}$$

The first group of functions $\bar{f}_{\xi j}(v,t)$ $(\xi = x,y,z;\ j = 1,2,\cdots)$ has the following differential properties

$$\frac{\partial^2 \bar{f}_{\xi j}(v,t)}{\partial v^2} = 0 \qquad (\xi = x,y,z;\ j = 1,2,\cdots) \tag{7}$$

The second group of functions $\hat{f}_{\xi k}(v,t)$ $(\xi = x,y,z; k = 1,2,\cdots)$ has the following differential properties

$$\frac{\partial^{2m} \hat{f}_{\xi k}(v,t)}{\partial v^{2m}} = \beta_{\xi k}^m \hat{f}_{\xi k}(v,t) \qquad (\xi = x,y,z; k = 1,2,\cdots; m = 1,2,3) \tag{8}$$

The third group of functions $\widetilde{f}_{\xi l}(v,t)$ $(\xi = x,y,z; l = 1,2,\cdots)$ has no any of the differential properties (7) and (8).

After decomposing the functions in the blending boundary constraints (1) into the above three groups of boundary functions, the blending boundary constraints (1) become

$$\begin{aligned}
&u=0 \quad && S_\xi(u,v,t)=\overline{C}_{\xi 1}+\hat{C}_{\xi 1}+\widetilde{C}_{\xi 1} && \partial S_\xi(u,v,t)/\partial u=\overline{C}_{\xi 2}+\hat{C}_{\xi 2}+\widetilde{C}_{\xi 2}\\
& && \partial^2 S_\xi(u,v,t)/\partial u^2=\overline{C}_{\xi 3}+\hat{C}_{\xi 3}+\widetilde{C}_{\xi 3} &&\\
&u=1 && S_\xi(u,v,t)=\overline{C}_{\xi 4}+\hat{C}_{\xi 4}+\widetilde{C}_{\xi 4} && \partial S_\xi(u,v,t)/\partial u=\overline{C}_{\xi 5}+\hat{C}_{\xi 5}+\widetilde{C}_{\xi 5} \qquad (9)\\
& && \partial^2 S_\xi(u,v,t)/\partial u^2=\overline{C}_{\xi 6}+\hat{C}_{\xi 6}+\widetilde{C}_{\xi 6} &&
\end{aligned}$$

$(\xi = x, y, z)$

If we decompose the mathematical functions $S_\xi(u,v,t)$ $(\xi = x, y, z)$ of the blending surface into the corresponding three parts: $\overline{S}_\xi = \overline{S}_\xi(u,v,t)$, $\hat{S}_\xi = \hat{S}_\xi(u,v,t)$ and $\widetilde{S}_\xi = \widetilde{S}_\xi(u,v,t)$, and substitute $S_\xi(u,v,t) = \overline{S}_\xi + \hat{S}_\xi + \widetilde{S}_\xi$ into Eq. (5), we reach

$$(\gamma\frac{\partial^6}{\partial u^6}+\eta\frac{\partial^6}{\partial u^4\partial v^2}+\lambda\frac{\partial^6}{\partial u^2\partial v^4}+\rho\frac{\partial^6}{\partial v^6})\left[\overline{S}_\xi(u,v,t)+\hat{S}_\xi(u,v,t)+\widetilde{S}_\xi(u,v,t)\right]=0 \qquad (10)$$

On the trimlines $u=0$ and $u=1$, $\overline{S}_\xi(u,v,t)$, $\hat{S}_\xi(u,v,t)$ and $\widetilde{S}_\xi(u,v,t)$ correspond to $\overline{C}_{\xi n}(v,t)$, $\hat{C}_{\xi n}(v,t)$ and $\widetilde{C}_{\xi n}(v,t)$, respectively. Solving Eq. (5) subjected to (1) can be transformed into solving each of the terms in the square bracket of Eq. (10) subjected to the blending boundary constraints consisting of the corresponding terms in Eq. (9).

As derived in Appendix A, the unknown functions $\overline{S}_\xi(u,v,t)$ are found to be:

$$\overline{S}_\xi(u,v,t)=\sum_j\sum_{n=1}^{6} g_n(u)\overline{a}_{\xi j,n}\,\overline{f}_{\xi j}(v,t) \qquad (\xi = x,y,z;\ \mathrm{j}=1,2,\cdots) \qquad (11)$$

where $g_n(u)$ $(n=1,2,\cdots,6)$ are determined by Eq. (A8), and $\overline{a}_{\xi j,n}$ and $\overline{f}_{\xi j}(v,t)$ are determined by the first one of Eq. (6).

As derived in Appendix B, the unknown functions $\hat{S}_\xi(u,v,t)$ are obtained as

$$\hat{S}_\xi(u,v,t)=\sum_k\Big[\hat{b}_{\xi k,1}e^{q_0u}+\hat{b}_{\xi k,2}e^{-q_0u}+e^{q_1u}\Big(\hat{b}_{\xi k,3}\cos q_2u+\hat{b}_{\xi k,4}\sin q_2u\Big)+e^{-q_1u}\Big(\hat{b}_{\xi k,5}\cos q_2u+\hat{b}_{\xi k,6}\sin q_2u\Big)\Big]\hat{f}_{\xi k}(v,t)$$
$$(\xi=x,y,z) \tag{12}$$

where the determination of the unknown constants q_0, q_1, q_2, and $\hat{b}_{\xi k,n}$ $(n=1,2,\cdots,6)$ is described in Appendix B, and $\hat{f}_{\xi k}(v,t)$ are determined by the second one of Eq. (6)

Unlike the unknown functions $\bar{S}_\xi(u,v,t)$ and $\hat{S}_\xi(u,v,t)$ whose exact closed form solutions are obtainable, the exact closed form solutions (CFS) for the unknown functions $\tilde{S}_\xi(u,v,t)$ do not exist. In Appendix C, we derive their approximate analytical solutions below

$$\tilde{S}_\xi(u,v,t)=\sum_l\sum_{n=1}^{6}\tilde{a}_{\xi l,n}g_n(u)-\sum_{m=1}^{M}\tilde{c}_{\xi l,m}\big[m\pi f_m(u)-\sin m\pi u\big]\tilde{f}_{\xi l}(v,t)$$
$$(\xi=x,y,z;\ l=1,2,\cdots) \tag{13}$$

where $g_n(u)$ is determined by Eq. (A8), $\tilde{a}_{\xi l,n}$ and $\tilde{f}_{\xi l}(v,t)$ are determined by the third one of Eq. (6), $\tilde{c}_{\xi l,m}$ are determined by Eq. (C12), and M indicates the total number of the sine terms. The bigger the value of M, the more accurate of the approximate analytical solution.

Putting the obtained $\bar{S}_\xi(u,v,t)$, $\hat{S}_\xi(u,v,t)$, and $\tilde{S}_\xi(u,v,t)$ together, we obtain the mathematical expression of blending surfaces. They will be used to investigate the accuracy, efficiency, and effects of the second partial derivatives and shape control

parameters in Section 5. The applications of the proposed approach in time-dependent and time-independent surface blending will be demonstrated in Section 6.

5 RESULTS AND DISCUSSION

In this section, we implement the proposed approach, compare it with the exact closed form solution to demonstrate its good accuracy and high efficiency and with the time-dependent C^1 continuous surface blending in [9] to investigate the differences between C^1 and C^2 continuities, discuss the influence of second partial derivatives on the continuity at timelines, and investigate shape control of C^2 continuous surface blending.

The obtained mathematical expressions (11), (12) and (13) of blending surfaces were implemented with C++ and OpenGL. All the examples were run on a same desktop with 3.5 GHz CPU.

5.1 Accuracy and Efficiency

First, we demonstrate good accuracy and high efficiency of the proposed approach by comparing it with the accurate closed form solution through creating a time-dependent blending surface between two separate elliptic cylinders represented with time-dependent primary surfaces. The primary surfaces for this example are

defined in Eqs. (2) and (3), and the blending boundary constraints are described in Eq. (4).

The functions in the blending boundary constraints (4) can be divided into two types, i. e., $\bar{S}_{\xi}(u,v,t)$ and $\hat{S}_{\xi}(u,v,t)$. In order to investigate the accuracy and efficiency, we use both the exact closed form solutions (12) and the approximate analytical solutions (13) to obtain the unknown functions $\hat{S}_{\xi}(u,v,t)$. Using the same geometric parameters $a=3.6$, $b=5.5$, $c=6.0$, $d=3.0$, $h_1=2.0$, $h_2=6.0$, and $h_3=20.0$, taking the trimlines to be at $u_0=0.4$ and $u_1=0.55$, and setting the shape control parameters to $\gamma=\eta=\lambda=\rho=1$, the time variable to $t=0.1$, and M in Eq. (13) to 10, 15, and 20, the blending surfaces $\mathbf{S}_M(u,v,t=0.1)$ obtained from the approximate analytical solution are depicted in Fig. 2 where M indicates the total terms used in Eq. (13).

Using the same geometric and shape control parameters, the blending surface $S_{CFS}(u,v,t=0.1)$ obtained from the exact closed form solution (12) is also shown in Fig. 2 where CFS indicates the closed form solution.

The first image of the second row of the figure shows the profile curves of the blending surface obtained from $M=10$, 15, and 20 of the proposed approach and the exact closed form solution, and the profile curves are magnified in the second and third images of the second row with the two innermost profile curves from $M=10$. The second row of Fig. 2 shows no visible difference between profile curves from $M=15$ and $M=20$ of the proposed approach and the closed form solution.

Next, we quantify the errors between the approximate analytical solution and the exact closed form solution. If p_i and q_i are used to indicate the i^{th} point on the blending surfaces respectively obtained from the developed approximate analytical solution and the exact closed form solution, i. e., $p_i = \mathbf{S}_M(u_i, v_i, t = 0.1)$ and $q_i = S_{CFS}(u_i, v_i, t = 0.1)$, the Euclidean distance between the i^{th} point on the two blending surfaces is $d(p_i, q_i)$ [25] . The errors between the proposed approximate analytical solution and the exact closed form solution are calculated with the following equations

$$E_1 = \max\{d(p_i, q_i)\} \qquad E_2 = \frac{1}{I}\sum_{i=1}^{I} d(p_i, q_i)$$
$$E_3 = \max\left\{\frac{d(p_i, q_i)}{D}\right\} \qquad E_4 = \frac{1}{I}\sum_{i=1}^{I} \frac{d(p_i, q_i)}{D} \tag{14}$$

In the equation, E_1, E_2, E_3, and E_4 indicate absolute maximum error, absolute average error, relative maximum error, and relative average error, respectively, I is the total number of all the points on a blending surface, and D is the maximum distance between two points of the blending surface with the same parametric values u but different parametric values v. The errors obtained from Eq. (14) are given in Table 1. The computational time (CPU) used to determine all the unknown constants and generate the blending surfaces with $M = 10$, 15 and 20 and four different quad meshes is also given in the same table where T1, T2, T3 and T4 stand for the computational time for the quad meshes with 51×51, 101×101, 151×151, and 201×201 vertices, respectively.

The data in Table 1 demonstrate good accuracy and high computational efficiency of the proposed approximate analytical solution. When M increases from 10 to 20, the relative average error (E_4) of the proposed approach decreases from 4.63×10^{-3} to 2.80×10^{-6}. With the increase of the total vertices, the computational time for both approximate analytical solution and exact closed form solution rises. When $M=10$, the approximate analytical solution is more efficient than the exact closed form solution for all the four meshes. When $M=20$, the computational time of the approximate analytical solution becomes larger than the exact closed form solution but still at the same order.

Unlike the exact closed form solution which is applicable to simple blending boundary constraints involving constants, sine and cosine functions, and exponential functions only, the developed approximate analytical solution is applicable to various complicated blending boundary constraints.

With the developed approach and setting the time variable $t=0$, 0.2, 0.4, 0.6, 0.8 and 1, the blending surfaces at these time instants are obtained and depicted in Fig. 3 where the first row is from the front view and the second row is from the side view.

The images shown in Fig. 3 indicate that at different time instants, the proposed approach always creates C^2 continuous blending surfaces to smoothly connect time-dependent primary surfaces together.

5.2 Comparison with Time-Dependent C^1 Continuous Surface Blending

In this subsection, we compare the C^2 continuous surface blending developed in this paper with the C^1 continuous surface blending introduced in [9] through a blending example. It creates a smooth transition between two time-dependent cylinders.

The parametric equations for the first cylinder are

$$x = ae^{t}\sin 2\pi v \qquad y = ae^{-t}\cos 2\pi v \qquad z = h_1 + h_2 u^2 \tag{15}$$

The parametric equations for the second cylinder are

$$x = be^{-t}\sin 2\pi v \qquad y = be^{t}\cos 2\pi v \qquad z = -h_3 u^3 \tag{16}$$

In the above equations (15) and (16), the geometric parameters are taken to be $a = 1.0$, $b = 0.8$, $h_1 = 2.0$, $h_2 = 3.0$, and $h_3 = 5.0$. The trimlines are at $u_0 = 0.2$ and $u_1 = 0.3$ where u_0 and u_1 stand for the isoparametric lines of the first and second cylinders, respectively.

The position functions and the first partial derivatives at the timelines required by the blending boundary constraints described in [9] can be derived from Eqs. (15) and (16). All the shape control parameters are set to 1, the total terms are $k = 10$. The C^1 continuous blending surface at the time instant t = 0 created by the approach proposed in [9] is depicted in Fig. 4(a), and the computational time (CPU) is 145 milliseconds.

With the approach proposed in this paper, the second partial derivatives at the trimlines are derived from Eqs. (15) and (16), and added to the blending boundary constraints. All the shape control parameters are also set to 1, the total terms are $M = 10$, and all the geometric parameters are kept unchanged. The C^2 continuous

blending surface at the time instant $t = 0$ created by the approach proposed in this paper is shown in Fig. 4(b), and the computational time (CPU) is 178 milliseconds.

Since the two approaches uses different partial differential equations (fourth-order vs sixth-order) and different blending boundary constraints (without and with the second partial derivatives), the shapes of the blending surfaces generated with the two different approaches are different and we cannot compare their shapes. Therefore, we compare the computational efficiency and how the second partial derivatives affect curvature continuity.

Although the approach proposed in this paper uses sixth-order partial differential equations and more blending boundary constraints, i. e., the second partial derivatives, the computational time for the two approaches is at the same order. Without the constraint of the second partial derivatives, the curvature continuity at the trimlines cannot be maintained as shown in Fig. 4(a). After applying the constraint of the second partial derivatives, good curvature continuity at the trimlines is achieved as shown in Fig. 4(b).

5.3 Effects of Second Partial Derivatives

Unlike the C^1 continuous surface blending presented in [9] which only maintains the continuities of the position functions and first partial derivatives at trimlines, the C^2 continuous surface blending developed in this paper introduces second partial derivatives at trimlines to achieve higher continuity. In this subsection, we will

demonstrate how second partial derivatives at trimlines affect the continuity between the blending surface and primary surfaces.

Still setting the time variable $t = 0$ and using the same position functions, and the first and second partial derivatives of x and y components for both the blending surface and primary surfaces at timelines as those determined by Eqs. (15) and (16), three different cases of the second partial derivatives of the z component are considered. For all the three cases, the z component of the primary surfaces and the blending surface always has the same position functions and first derivatives at the trimlines. For the first case, the blending surface and primary surfaces have the same second partial derivatives $-2h_2$ at the trimline $u = 0$ and $-6h_3u_1$ at the trimline $u = 1$, and the obtained blending surface is shown in Fig. 5(a). For the second case, the blending surface increases its second partial derivative to $-10h_2$ at the trimline $u = 0$ and $-18h_3u_1$ at the trimline $u = 1$, and the obtained blending surface is indicated in Fig. 5(b). For the third case, the blending surface further raises its second partial derivative to $-20h_2$ at the trimline $u = 0$ and $-36h_3u_1$ at the trimline $u = 1$, and the generated blending surface is depicted in Fig. 5(c). In the figure, the images in the bottom row show different shapes of the blending surface only. They are used to demonstrate how the second partial derivatives affect the continuity at the trimlines.

It can be seen from the images that when the blending surface and primary surfaces have the same second partial derivatives at the trimlines, good continuity between the blending surface and the primary surfaces is obtained as shown in Fig. 5(a). When the second partial derivatives of the blending surface and primary surfaces at

trimlines are different, poor continuity from the blending surface to primary surfaces occurs as indicted in Fig. 5(b). If the difference of the second partial derivatives between the blending surface and primary surfaces is bigger, the continuity between the blending surface and primary surfaces becomes worse as shown in Fig. 5(c).

5.4 Shape Control of Blending Surfaces

One of the main advantages of the proposed approach is it provides effective shape control to obtain different shapes of blending surfaces. In this subsection, we investigate how to use different shape control parameters to create different shapes of blending surfaces.

In order to generate different shapes of primary and blending surfaces, the geometric parameters in the primary surfaces (2) and (3) and the blending boundary constraints (4) are changed to: $a = 2.6$, $b = 4.5$, $c = 5.0$, $d = h_1 = 2.0$, $h_2 = 3.0$, and $h_3 = 5.0$, and the trimlines are changed to $u_0 = 0.5$ for the top surface and $u_1 = 0.4$ for the bottom surface. If we do not want to use the shape control parameters to manipulate blending surfaces, we can simply set all the shape control parameters to 1, i. e., $\gamma = \eta = \lambda = \rho = 1$. The obtained blending surfaces at the time instants $t = 0.2$, 0.4 and 0.6 are shown in Fig. 6.

If we want to use the shape control parameters to create different shapes of blending surfaces and select the required ones from them, we can set shape control

parameters to different values. In what follows, we will investigate the effects of the shape parameters γ, η, λ, and ρ on the blending surface.

5.4.1 Effects of Shape Control Parameter γ

Firstly, we investigate how to use the shape control parameter γ to achieve different shapes of the blending surface. To this aim, we keep the shape control parameters $\eta = \lambda = \rho = 1$ unchanged, and set the time variable $t = 0$ and the shape control parameter γ to different values shown in Fig. 7. With the developed approximate analytical solution, different shapes of the blending surface are obtained and depicted in the same figure where the last image shows the profile curves of different shapes of the a same blending surface.

Examining the shapes of the blending surface in Fig. 7, we can conclude: 1) when the shape control parameter γ changes from -10 to -2.6, the concave blending surface becomes straight and bigger, 2) with further changes from -2.6 to -2, the middle part of the blending surface becomes more and more convex.

5.4.2 Effects of Shape Control Parameter η

Secondly, we keep the shape control parameters $\gamma = \lambda = \rho = 1$, and set η to different values shown in Fig. 8. The obtained shapes of the blending surface and their profile curves are shown in the same figure.

The blending surfaces in Fig. 8 indicate that when the shape control parameter η changes from -11.0 to -7.0, the middle part of the blending surface first becomes straight, then becomes more concave and smaller. With further changes from -7.0 to -4.5, the middle part of the blending surface is changed into a shape like the frustum of a cone first, and finally becomes most concave at $\eta = -4.5$.

5.4.3 Effects of Shape Control Parameter λ

Thirdly, we keep the shape control parameters $\gamma = \eta = \rho = 1$ unchanged, and set the shape control parameter λ to different values shown in Fig. 9. The obtained shapes of the blending surface and their profile curves are also given in the same figure.

From Fig. 9, we found that the middle part of the blending surface is most concave at $\lambda = -0.5$ among the λ values between -0.5 and 7.0. When λ changes from -0.5 to 7.0, the blending surface becomes less concave until it becomes a cylinder-like shape at $\lambda = 7.0$.

5.4.4 Effects of Shape Control Parameter ρ

Finally, we examine how the shape control parameter ρ affects the shape of the blending surface. We keep the shape control parameters $\gamma = \eta = \lambda = 1$, and set the shape control parameter ρ to different values shown in Fig. 10. The generated shapes of the blending surface and their profile curves are also depicted in the same figure.

The blending surfaces shown in Fig. 10 indicate that when the shape control parameter ρ changes from -1.5 to -0.7, the straight middle part of the blending surface first becomes convex, and then changes back to the frustum of a cone but with a bigger cross-section size. When the shape control parameter ρ changes from -0.7 to 3.0, the blending surface becomes more and more concave and reaches most concave at $\rho = 3.0$.

The above discussions indicate that all the four shape control parameters have a great influence on the shape of the blending surface. They can be developed into useful user handles to effectively control the shape of the blending surface.

6 APPLICATIONS

In this section, we first use the developed approximate analytical solution to create two time-dependent blending surfaces of C2 continuity. Then, we employ the developed approximate analytical solution to create some time-independent blending surfaces frequently met in engineering applications.

6.1 Time-Dependent Surface Blending

First, we investigate surface blending between linearly varying primary surfaces. Then, we create a blending surface between non-linearly varying primary surfaces.

6.1.1 Surface Blending between Linearly Varying Primary Surfaces

For the first application example, two primary surfaces change their shapes linearly. The first primary surface varies from an open surface to a closed one, and the second primary surface changes from a plane to a cone shaped frustum.

The parametric equations of the first primary surfaces are constructed as

$$\begin{aligned} x &= (1-t)\left[b_1 \sinh(a_1 v + a_2) + b_2(1+u^3)\sin(a_3 v)\right] + b_3 t\cos(-v) \\ y &= (1-t)\left[b_4 \cosh(a_4 v) + b_2(1+u^3)\cos(a_3 v)\right] + b_5 t\sin(-v) \\ z &= (1-t)(h_0 + b_6 + e^u) + (h_1 + h_2 u^2)t \end{aligned} \tag{17}$$

The parametric equations for the second primary surface are constructed as

$$\begin{aligned} x &= (0.8+u)(1-t)b_6 \sin(a_5 v) + b_7 t\cos(-v) \\ y &= 0.8(1-t)b_6 \cos(a_5 v) + b_8 t\sin(-v) \\ z &= (1-t)h_3 + [h_4 + h_5 \sinh(-u)]t \end{aligned} \tag{18}$$

The geometric parameters in the above Eqs. (17) and (18) are taken to be: $a_1 = a_2 = b_1 = 0.1$, $a_3 = a_5 = b_6 = h_2 = h_5 = 0.1$, $a_4 = b_4 = 0.3$, $b_2 = 1.5$, $b_3 = 1.2$, $b_5 = 0.8$, $b_6 = 1.6$, $b_7 = 0.5$, $b_8 = 0.7$, $h_0 = 0.75$, $h_1 = 1.7$, and $h_3 = h_4 = -0.5$. The trimlines are taken to be at the isoparametric lines $u_0 = u_1 = 0$ where u_0 and u_1 stand for the isoparametric lines of the first and second primary surfaces, respectively.

From the parametric equations of the two primary surfaces, we can obtain the position functions, and the first and second partial derivatives of the first surface at $u_0 = 0$ and the second surface at $u_1 = 0$. They are taken to be the boundary constraints of the blending surface at its isoparametric lines $u = 0$ and $u = 1$, respectively. With the

developed approach, the C^2 continuous blending surface is generated whose shapes at the time $t = i/5$ ($i = 0,1,2,\cdots,5$) are depicted in Fig. 11.

This example indicates that although the two primary surfaces continuously change their shapes, the proposed approach creates a blending surface which connects the varying shapes together with C^2 continuity.

6.1.2 Surface Blending between Nonlinearly Varying Primary Surfaces

For the second application example, two primary surfaces change their shapes following a nonlinear sine variation. The first primary surface initially has some wrinkles, and finally becomes the frustum of a smooth inclined circular cone. The second primary surface changes from a cone-shaped elliptic cylinder to an inclined plane.

The parametric equations of the first primary surfaces are constructed as

$$\begin{aligned} x &= [(1-\sin(\pi t/2)](1+k_1u^2)[r_0\cos v + r_1\cos(kv)] + r\sin(\pi t/2)(k_2+u)^2\cos v \\ y &= [(1-\sin(\pi t/2)](1+k_1u^2)[r_0\sin v + r_1\sin(kv)] + r\sin(\pi t/2)(k_2+u)^2\sin v \\ z &= [(1-\sin(\pi t/2)](h_0+h_1u) + \sin(\pi t/2)[h_2+h_3(k_2+u)+h_4\cos v] \end{aligned} \tag{19}$$

The parametric equations for the second primary surface are constructed as

$$\begin{aligned} x &= a[(1-\sin(\pi t/2)](k_3+u)\cos v + r_2\sin(\pi t/2)(k_4+u)\cos(-\alpha)\cos v \\ y &= b[(1-\sin(\pi t/2)](k_3+u)\sin v + r_2\sin(\pi t/2)(k_4+u)\sin v \\ z &= [(1-\sin(\pi t/2)][h_5-h_6(k_5+u)] + \sin(\pi t/2)[h_7-h_8(k_4+u)\sin(-\beta)\cos v] \end{aligned} \tag{20}$$

The geometric parameters in the above Eqs. (19) and (20) are taken to be: $a = 0.64$, $b = k_2 = 0.6$, $h_0 = 0.3$, $h_1 = 1.5$, $h_2 = h_5 = -1.0$, $h_3 = r_2 = 2.0$, $h_4 = 0.5$, $h_6 = 1.5$, $h_7 = -2.0$, $h_8 = 2.0$, $k = 12.0$, $k_1 = 1$, $k_3 = 2.5$, $k_4 = 0.8$, $k_5 = 0.5$, $r = 0.8$, $r_0 = 0.9$,

$r_1 = 0.05$, and $\alpha = -20\pi/180$. For both primary surfaces, the trimlines are at $u_0 = u_1 = 0$. Using the proposed method, different shapes of the blending surface at the time instants $t = i/5$ ($i = 0,1,2,\cdots,5$) are depicted in Fig. 12.

This example also demonstrates the capacity of our proposed approach in connecting two time-dependent primary surfaces together with C^2 continuity.

6.2 Time-Independent Surface Blending

The proposed approach is also effective in time-independent surface blending. In this subsection, we will present some examples to demonstrate this and its engineering applications.

Blending surfaces which blend NURBS surfaces, intersecting planes, intersecting cylinders, and a cylinder to a plane are most common in mechanical engineering. In what follows, we will investigate how to use the developed approach to tackle these surface blending problems.

6.2.1 Surface Blending between NURBS Surfaces

A NURBS surface $\mathbf{S}(u,v) = \begin{bmatrix} S_x(u,v) & S_y(u,v) & S_z(u,v) \end{bmatrix}^T$ is a bivariate vector-valued piecewise rational function of the form

$$\mathbf{S}(u,v) = \sum_{i=0}^{n}\sum_{j=0}^{m} N_{i,p}(u) N_{j,q}(v) w_{ij} \mathbf{P}_{ij} \Big/ \bar{S}(u,v) \tag{21}$$

where

$$\bar{S}(u,v)=\sum_{i=0}^{n}\sum_{j=0}^{m}N_{i,p}(u)N_{j,q}(v)w_{ij} \tag{22}$$

and

$$\begin{aligned}
&N_{k,0}(t)=\begin{cases}1 & \text{if}\left(t_i\le t<t_{i+1}\right)\\ 0 & otherwise\end{cases}\\
&N_{k,l}(t)=\frac{t-t_i}{t_{k+l}-t_k}N_{k,l-1}(t)+\frac{t_{k+l+1}-t}{t_{k+l+1}-t_{k+1}}N_{k+1,l-1}(t) \qquad (23)\\
&(k=i,\,j;l=p,q;t=u,v)
\end{aligned}$$

In the equation, p and q are the degrees in the u and v directions, respectively, $\mathbf{P}_{ij}=\begin{bmatrix}P_{xij} & P_{yij} & P_{zij}\end{bmatrix}^T$ are the control points, and w_{ij} are the weights.

When two NURBS surfaces $\mathbf{S}_1(u,v)$ and $\mathbf{S}_2(u,v)$ are to be smoothly blended together by a blending surface $\mathbf{S}(u,v)$ at $u=0$ of $\mathbf{S}_1(u,v)$ and $u=1$ of $\mathbf{S}_2(u,v)$, we first obtain $\mathbf{C}_1(v)=\mathbf{S}_1(u=0,v)$ and $\mathbf{C}_4(v)=\mathbf{S}_2(u=1,v)$. Then we derive the first and second partial derivatives of the two NURBS surfaces, and obtain $\mathbf{C}_2(v)=\partial\mathbf{S}_1(u=0,v)/\partial u$, $\mathbf{C}_3(v)=\partial^2\mathbf{S}_1(u=0,v)/\partial u^2$, $\mathbf{C}_5(v)=\partial\mathbf{S}_2(u=1,v)/\partial u$, and $\mathbf{C}_6(v)=\partial^2\mathbf{S}_2(u=1,v)/\partial u^2$.

Substituting the obtained $\mathbf{C}_i(v)$ ($i=1,2,\cdots,6$) into Eqs. (C9) and (C10), and solving Eq. (C12), we obtain all the unknown constants and the mathematical expression (13) of the blending surface.

In order to tackle various NURBS surface blending problems, we considered a general case where 16 control points and 8 knots were used to generate the first cubic NURBS surface $\mathbf{S}_1(u,v)$ highlighted in grey in Fig. 13, and 25 control points and 10 knots were used to generate the second quartic NURBS surface $\mathbf{S}_2(u,v)$ highlighted in light

blue. The obtained blending surface $\mathbf{S}(u,v)$ was shown in blue in the same figure where the two images were obtained from two different viewpoints of a same blending surface.

The images in Fig. 13 show smooth transition from the blending surface to the two NURBS surfaces. It demonstrates the effectiveness of the proposed approach in blending NURBS surfaces with C^2 continuity.

6.2.2 Surface Blending between Intersecting Planes

Generating a smooth transition surface between two intersecting planes frequently appears in engineering design or manufacturing process to reduce stress concentration at the joint between the two planes. For this surface blending problem, the boundary constraints can be formulated as:

$$\begin{array}{llll} u=0 & x=0 & y=h_0+h_1v & z=pv \\ & \dfrac{\partial x}{\partial u}=0 & \dfrac{\partial y}{\partial u}=-(h_2+h_3v) & \dfrac{\partial z}{\partial u}=0 \\ & \dfrac{\partial^2 x}{\partial u^2}=0 & \dfrac{\partial^2 y}{\partial u^2}=-\eta(h_2+h_3v) & \dfrac{\partial^2 z}{\partial u^2}=0 \\ u=1 & x=s_0+s_1v & y=0 & z=pv \\ & \dfrac{\partial x}{\partial u}=s_2+s_3v & \dfrac{\partial y}{\partial u}=0 & \dfrac{\partial z}{\partial u}=0 \\ & \dfrac{\partial^2 x}{\partial u^2}=0 & \dfrac{\partial^2 y}{\partial u^2}=0 & \dfrac{\partial^2 z}{\partial u^2}=0 \end{array} \tag{24}$$

Setting the parameters in Eq. (24) to: $h_0=0.9$, $h_1=-0.4$, $h_2=1.1$, $h_3=s_3=0.01$, $s_0=1$, $s_1=-0.5$, $s_2=1.2$ and $p=2$, we obtain the blending surface

demonstrated in Fig. 14(a) for $\eta = -10$ and Fig. 14(b) for $\eta = 0$ where Figs. 14(c) and 14(d) show a very small local part of the blending surfaces depicted in Figs. 14(a) and 14(b). It can be seen that the second derivative in Eq. (24) determined by $\eta = 0$ creates a smoother blending surface than that determined by $\eta = -10$.

The proposed approach is advantageous over constant and variable radius rolling-ball blends since it can achieve different levels of smoothness at trimlines and different shapes of blending surfaces. In contrast, constant and variable radius rolling-ball blends cannot change both the smoothness and shape of the blending surface once the trimlines are specified.

6.2.3 Surface Blending between Intersecting Cylinders

Creating a smooth transition between intersecting cylinders is also very common in engineering design and manufacturing. When blending two intersecting cylinders with C^2 continuity, the boundary constraints can be written as

$$\begin{array}{llll}
u=0 & x = s\cos v & y = s\sin v & z = f_2(v) \\
 & \dfrac{\partial x}{\partial u} = 0 & \dfrac{\partial y}{\partial u} = 0 & \dfrac{\partial z}{\partial u} = f_3(v) \\
 & \dfrac{\partial^2 x}{\partial u^2} = 0 & \dfrac{\partial^2 y}{\partial u^2} = 0 & \dfrac{\partial^2 z}{\partial u^2} = f_4(v) \\
u=1 & x = (s+l_1)\cos v & y = (s+l_1)\sin v & z = f_5(v) \\
 & \dfrac{\partial x}{\partial u} = (s+l_1)\cos v & \dfrac{\partial y}{\partial u} = (s+l_1)\sin v & \dfrac{\partial z}{\partial u} = f_6(v) \\
 & \dfrac{\partial^2 x}{\partial u^2} = 0 & \dfrac{\partial^2 y}{\partial u^2} = 0 & \dfrac{\partial^2 z}{\partial u^2} = f_7(v)
\end{array} \tag{25}$$

where

$$f_2(v)=\sqrt{f_0(v)} \qquad f_3(v)=-(r+k_1)\Big/\sqrt{f_0(v)}$$
$$f_4(v)=1\Big/\sqrt{f_0(v)}-(r+k_1)^2\Big/\sqrt[3]{f_0(v)} \qquad f_5(v)=\sqrt{f_1(v)} \tag{26}$$
$$f_6(v)=-(s+l_1)\cos^2 v\Big/\sqrt{f_1(v)} \qquad f_7(v)=\cos^2 v\Big/\sqrt{f_1(v)}-(s+l_1)^2\cos^4 v\Big/\sqrt[3]{f_1(v)}$$

and

$$f_0(v)=(r+k_1)^2-s^2\cos^2 v \qquad f_1(v)=r^2-(s+l_1)^2\cos^2 v \tag{27}$$

Setting the shape parameters to $\gamma=\eta=\lambda=\rho=1$ and geometric parameters to $s=0.7$, $l_1=0.3$, $r=1.2$, and $k_1=0.5$, we obtain the blending surface depicted in Fig. 15(a) and Fig. 15(b) where $\partial z/\partial u=f_3(v)$ and $\partial^2 z/\partial u^2=f_4(v)$.

How the first and second partial derivatives affect the smoothness and the shape of the blending surface can be obtained by scaling them. Setting $\partial z/\partial u=0.01f_3(v)$ and keeping $\partial^2 z/\partial u^2=f_4(v)$ unchanged, we obtain the blending surface depicted in Fig. 15(c). If we fix $\partial z/\partial u=f_3(v)$ but set $\partial^2 z/\partial u^2=10f_4(v)$, the blending surface shown in Fig. 15(d) is generated. These images demonstrate the effectiveness of the first and second partial derivatives in changing the smoothness and the shape of blending surfaces.

6.2.4 Surface Blending between a Cylinder and a Plane

The final example is to create a time-independent C^2 continuous blending surface smoothly connecting a cylinder to a plane. It is widely applied in mechanical components and parts such as a transmission yoke - drive shaft shown in Fig. 16(a)

where the blending between the cylinders and planes in the highlighted region is required.

Due to limitations of space, the blending boundary constraints are not given here. The obtained blending surface is shown in (b) and (c) of Fig. 16 where (b) is rendered with a same colour and (c) is rendered with three different colours.

7 CONCLUSIONS AND FUTURE WORK

In this paper, we have developed a new surface blending method to create a C^2 continuous blending surface. The proposed mathematical model can tackle both time-dependent and time-independent parametric surfaces, and the developed approximate analytical solution is simple and easy to use.

We investigated the accuracy, efficiency, effects of the second derivatives, the comparison with the time-dependent C^1 continuous surface blending given in [9], and how different shape control parameters affect the shape of time-dependent blending surfaces. It was found: 1) the proposed approach has good accuracy and high efficiency, 2) the second partial derivatives play an important role in achieving good continuity, 3) all the shape control parameters have a strong impact on the shape of the blending surface, and can be developed into effective shape control handles to achieve the required shapes of blending surfaces. We have also presented some examples of time-dependent and time-independent surface blending to demonstrate engineering applications of the proposed approach.

One of the main advantages of the proposed approach is the shape control parameters can be optimized to: 1) minimize stress concentrations in engineering applications, and 2) create user's specified shapes for aesthetic or other requirements. Stress concentrations are related to the curvature of blending surfaces between primary surfaces such as two intersecting planes to be smoothly connected. Small curvature causes low stress concentrations. Therefore, minimizing stress concentrations is to find optimal shape control parameters which minimize the curvature of blending surfaces. In order to create user's specified shapes, one or more profile curves will be first drawn by users. The difference between the user's drawn profile curves and the corresponding ones of blending surfaces is minimized to obtain optimal shape control parameters and create the user's specified shapes of blending surfaces. We will investigate these important topics in the future.

REFERENCES

[1] Rossignac, J. R., Requicha, A. A. G., 1984, "Constant-radius blending in solid modeling," Comp. Mech. Eng. **3**, pp. 65-73.

[2] Vida, J., Martin, R. R., Varady T., 1994 "A survey of blending methods that use parametric surfaces," Comput. Aided Des. **26**(5), pp. 341-365.

[3] Rockwood, A. P., 1989 "The displacement method for implicit blending surfaces in solid models," ACM Trans. Graph. **8**(4), pp. 279-297.

[4] Filip, D. J., 1989 "Blending parametric surfaces," ACM Trans. Graph. **8**(3), pp. 164-173.

[5] Aumann, G., 1995 "Curvature continuous connections of cones and cylinders," Comput. Aided Des. **27**(4), pp. 293-301.

[6] Tosun, E., Gingold, Y. I., Reisman, J., Zorin, D., 2007 “Shape optimization using reflection lines,” Proceedings of the Fifth Eurographics Symposium on Geometry Processing, Eurographics Association, pp. 193-202.

[7] Pegna, J., Wolter, F.-E., 1992 “Geometrical criteria to guarantee curvature continuity of blend surfaces,” J. Mech. Des. ASME **114**, pp. 201-210.

[8] Shen, X., Avital, E., Rezaienia, M. A., Paul, G., Korakianitis, T. 2017 “Computational methods for investigation of surface curvature effects on airfoil layer behavior,” J. Algorithms Comput. Technol. **11**(1), pp. 68-82.

[9] You, L. H., Ugail, H., Zhang, J. J., 2012, “Controllable C^1 continuous blending of time-dependent parametric surfaces,” Vis. Comput. **28**, pp. 573-583.

[10] Kiciak, P., 2011 “Bicubic B-spline blending patches with optimized shape,” Comput. Aided Des. **43**, pp. 133-144.

[11] Dahl, H. E. I., Krasauskas, R., 2012 “Rational fixed radius rolling ball blends between natural quadrics,” Comput. Aided Geom. Des. **29**, pp. 691-706.

[12] Lukács, G., 1998 “Differential geometry of G1 variable radius rolling ball blend surfaces,” Comput. Aided Geom. Des. **15**, pp. 585-613.

[13] Hatna, A., Grieve, R. J., Broomhead, P. 2001 “Surface blending for machining purposes: A brief survey and application for machining compound surfaces,” P. I. Mech. Eng. B.-J. Eng. **215**(10), pp. 1397-1408.

[14] Hoffmann, C., Hopcroft, J., 1986 “Quadric blending surfaces,” Comput. Aided Des. **18**(6), pp. 301-306.

[15] Hoffmann, C., Hopcroft, J., 1987 “The potential method for blending surfaces and corners,” in Geometric Modeling: Algorithms and New Trends, eds. G. E. Farm (SIAM, USA, 1987), pp. 347-365.

[16] Ohkura, K., Kakazu, Y., 1992 “Generalization of the potential method for blending three surfaces,” Comput. Aided Des. **24**(11), pp. 599-609.

[17] Shi, K.-L., Yong, J.-H., Sun, J.-G., 2010 “Filling n-sided regions with triangular Coons B-spline patches,” Vis. Computer. **26**, pp. 791-780.

[18] Zhou, P. 2010 “Polyhedral vertex blending with setbacks using rational S-patches,” Comput. Aided Geom. Des. **27**, pp. 233-244.

[19] Krasauskas, R. 2008, “Branching blend of natural quadrics based on surfaces with rational offsets,” Comput. Aided Geom. Des. **25**, pp. 332-341.

[20] Bloor, M. I. G., Wilson, M. J., 1989 “Generating blend surfaces using partial differential equations,” Comput. Aided Des. **21**(3), pp. 165-171.

[21] Bloor, M. I. G., Wilson, M. J., Hagen, H., 1995 “The smoothing properties of variational schemes for surface design,” Comput. Aided Geom. Des. **12**(4), pp. 381-394.

[22] Brown, J. M., Wilson, M. J., Bloor, M. S., Wilson, M. J. 1998 “The accuracy of B-spline finite element approximations to PDE surfaces,” Comput. Methods Appl. Mech. Eng. **158**(3-4), pp. 221-234.

[23] Zhang, J. J., You, L. H., 2002 “PDE based surface representation - vase design,” Comput. Gr. **26**, pp. 89-92.

[24] Bloor, M. I. G., Wilson, M. J., 1996 “Spectral approximations to PDE surfaces,” Comput. Aided Des. **28**(2), pp. 145-152.

[25] Mora, H., Mora-Pascual, J. M., Garca-Garca, A., Martnez-Gonzlez, P., 2016, “Computational analysis of distance operators for the iterative closest point algorithm,” Plos One **11**(10), e0164694.

APPENDIX A: DETERMINATION OF $\bar{S}_\xi = \bar{S}_\xi(u,v,t)$

For the first group of boundary functions $\bar{f}_{ij}(v,t)\ \ (i=1,2,\cdots)$, the corresponding mathematical expressions of the blending surface can be taken to be

$$\bar{S}_\xi(u,v,t) = \sum_j H_{ij}(u)\,\bar{f}_{ij}(v,t) \qquad (\xi = x,y,z;\ \mathrm{j}=1,2,\cdots) \tag{A1}$$

The partial differential equations (10) corresponding to the mathematical expressions $\bar{S}_\xi(u,v,t)$ are

$$(\gamma\frac{\partial^6}{\partial u^6} + \eta\frac{\partial^6}{\partial u^4\partial v^2} + \lambda\frac{\partial^6}{\partial u^2\partial v^4} + \rho\frac{\partial^6}{\partial v^6})\bar{S}_\xi(u,v,t) = 0 \tag{A2}$$

The blending boundary constraints (9) corresponding to the mathematical expressions $\bar{S}_{\xi}(u,v,t)$ are

$$
\begin{aligned}
u=0 \qquad & \bar{S}_{\xi}(u,v,t)=\sum_{j}\bar{a}_{\xi j,1}\bar{f}_{\xi j}(v,t) \qquad && \partial\bar{S}_{\xi}(u,v,t)/\partial u=\sum_{j}\bar{a}_{\xi j,2}\bar{f}_{\xi j}(v,t) \\
& \partial^{2}\bar{S}_{\xi}(u,v,t)/\partial u^{2}=\sum_{j}\bar{a}_{\xi j,3}\bar{f}_{\xi j}(v,t) && \\
u=1 \qquad & \bar{S}_{\xi}(u,v,t)=\sum_{j}\bar{a}_{\xi j,4}\bar{f}_{\xi j}(v,t) \qquad && \partial\bar{S}_{\xi}(u,v,t)/\partial u=\sum_{j}\bar{a}_{\xi j,5}\bar{f}_{\xi j}(v,t) \\
& \partial^{2}\bar{S}_{\xi}(u,v,t)/\partial u^{2}=\sum_{j}\bar{a}_{\xi j,6}\bar{f}_{\xi j}(v,t) && \\
(\xi=x,y,z) &
\end{aligned}
\tag{A3}
$$

Substituting Eq. (A1) into (A2) and considering the differential properties (7) and the boundary constraints (A3), we obtain

$$
\frac{\partial^{6}\bar{H}_{\xi j}(u)}{\partial u^{6}}=0 \qquad (\xi=x,y,z;\ j=1,2,\cdots) \tag{A4}
$$

subjected to the following boundary constraints

$$
\begin{aligned}
u=0 \qquad & \bar{H}_{\xi j}(u)=\bar{a}_{\xi j,1} \qquad \partial\bar{H}_{\xi j}(u)/\partial u=\bar{a}_{\xi j,2} \qquad \partial^{2}\bar{H}_{\xi j}(u)/\partial u^{2}=\bar{a}_{\xi j,3} \\
u=1 \qquad & \bar{H}_{\xi j}(u)=\bar{a}_{\xi j,4} \qquad \partial\bar{H}_{\xi j}(u)/\partial u=\bar{a}_{\xi j,5} \qquad \partial^{2}\bar{H}_{\xi j}(u)/\partial u^{2}=\bar{a}_{\xi j,6} \\
(\xi=x,y,z;\ j=1,2,\cdots) &
\end{aligned}
\tag{A5}
$$

The solution to the sixth-order ordinary differential equation (A4) can be taken to be

$$
\bar{H}_{\xi j}(u)=\sum_{n=0}^{5}\bar{b}_{\xi j,n}u^{n} \qquad (\xi=x,y,z;\ j=1,2,\cdots) \tag{A6}
$$

where $\bar{b}_{\xi j,n}$ $(n=1,2,\cdots,6)$ are unknown constants.

Equations (A6) have exactly satisfied the sixth-order ordinary differential equation (A4). Substituting Eq. (A6) into the boundary constraints (A5), all the unknown

constants $\bar{b}_{\xi j,n}$ are determined. Introducing the determined unknown constants $\bar{b}_{\xi j,n}$ into (A6), and then substituting (A6) into (A1), we obtain

$$\bar{S}_{\xi}(u,v,t)=\sum_{j}\sum_{n=1}^{6}g_n(u)\bar{a}_{\xi j,n}\bar{f}_{\xi j}(v,t) \qquad (\xi=x,y,z;\ \mathrm{j}=1,2,\cdots) \tag{A7}$$

where

$$\begin{aligned} &g_1(u)=1-10u^3+15u^4-6u^5 && g_2(u)=(1-6u^2+8u^3-3u^4)u \\ &g_3(u)=(0.5-1.5u+1.5u^2-0.5u^3)u^2 && g_4(u)=(10-15u+6u^2)u^3 \\ &g_5(u)=(-4+7u-3u^2)u^3 && g_6(u)=(0.5-u+0.5u^2)u^3 \end{aligned} \tag{A8}$$

APPENDIX B: DETERMINATION OF $\hat{S}_{\xi}(u,v,t)$

For the second group of functions $\hat{f}_{\xi k}(v,t)$ $(k=1,2,\cdots)$, the corresponding mathematical expressions of the blending surface can be taken to be

$$\hat{S}_{\xi}(u,v,t)=\sum_{k}\hat{H}_{\xi k}(u)\,\hat{f}_{\xi k}(v,t) \qquad (\xi=x,y,z) \tag{B1}$$

The partial differential equations (10) corresponding to the mathematical expressions $\hat{S}_{\xi}(u,v,t)$ are

$$(\gamma\frac{\partial^6}{\partial u^6}+\eta\frac{\partial^6}{\partial u^4\partial v^2}+\lambda\frac{\partial^6}{\partial u^2\partial v^4}+\rho\frac{\partial^6}{\partial v^6})\hat{S}_{\xi}(u,v,t)=0 \tag{B2}$$

The blending boundary constraints (9) corresponding to the mathematical expressions $\hat{S}_{\xi}(u,v,t)$ are

$$
\begin{aligned}
u=0 \qquad & \hat{S}_\xi(u,v,t)=\sum_k \hat{a}_{\xi k,1}\hat{f}_{\xi k}(v,t) && \partial\hat{S}_\xi(u,v,t)\big/\partial u=\sum_k \hat{a}_{\xi k,2}\hat{f}_{\xi k}(v,t)\\
& \partial^2\hat{S}_\xi(u,v,t)\big/\partial u^2=\sum_k \hat{a}_{\xi k,3}\hat{f}_{\xi k}(v,t) &&\\
u=1 \qquad & \hat{S}_\xi(u,v,t)=\sum_k \hat{a}_{\xi k,4}\hat{f}_{\xi k}(v,t) && \partial\hat{S}_\xi(u,v,t)\big/\partial u=\sum_k \hat{a}_{\xi k,5}\hat{f}_{\xi k}(v,t)\\
& \partial^2\hat{S}_\xi(u,v,t)\big/\partial u^2=\sum_k \hat{a}_{\xi k,6}\hat{f}_{\xi k}(v,t) &&
\end{aligned}
\tag{B3}
$$

Substituting Eq. (B1) into (B2) and considering the differential properties (8) and the boundary constraints (B3), we obtain

$$
\left(\gamma\frac{\partial^6}{\partial u^6}+\eta\beta_{\xi k}\frac{\partial^4}{\partial u^4}+\lambda\beta_{\xi k}^2\frac{\partial^2}{\partial u^2}+\rho\beta_{\xi k}^3\right)\hat{H}_{\xi k}(u)=0 \qquad (\xi=x,y,z;k=1,2,\cdots) \tag{B4}
$$

subjected to the following boundary constraints

$$
\begin{aligned}
u=0 \qquad & \hat{H}_{\xi k}(u)=\hat{a}_{\xi k,1} \qquad \partial\hat{H}_{\xi k}(u)\big/\partial u=\hat{a}_{\xi k,2} \qquad \partial^2\hat{H}_{\xi k}(u)\big/\partial u^2=\hat{a}_{\xi k,3}\\
u=1 \qquad & \hat{H}_{\xi k}(u)=\hat{a}_{\xi k,4} \qquad \partial\hat{H}_{\xi k}(u)\big/\partial u=\hat{a}_{\xi k,5} \qquad \partial^2\hat{H}_{\xi k}(u)\big/\partial u^2=\hat{a}_{\xi k,6}\\
(\xi=x,y,z;k=1,2,\cdots) &
\end{aligned}
\tag{B5}
$$

The closed form solution of the sixth-order ordinary differential equation (B4) subjected to the boundary constraints (B5) is obtainable. Due to the different combinations of γ, η, λ, ρ, and $\beta_{\xi k}$, the closed form solution has many different forms. For the shape control parameters $\gamma=\eta=\lambda=\rho=1$, and $\beta_{\xi k}=-4\pi^2$, the closed form solution has the form of

$$
\begin{aligned}
&\hat{S}_\xi(u,v,t)=\sum_k\Big[\hat{b}_{\xi k,1}e^{q_0u}+\hat{b}_{\xi k,2}e^{-q_0u}+e^{q_1u}\left(\hat{b}_{\xi k,3}\cos q_2u+\hat{b}_{\xi k,4}\sin q_2u\right)+e^{-q_1u}\left(\hat{b}_{\xi k,5}\right.\\
&\left.\cos q_2u+\hat{b}_{\xi k,6}\sin q_2u\right)\Big]\hat{f}_{\xi k}(v,t)\\
&(\xi=x,y,z)
\end{aligned}
\tag{B6}
$$

where q_0, q_1 and q_2 are determined by substituting Eq. (B6) into the sixth-order partial differential equation (B2), and $\hat{b}_{\xi k,n}$ $(n=1,2,\cdots,6)$ are determined by substituting Eq. (B6) into the boundary constraints (B5).

APPENDIX C: DETERMINATION OF $\widetilde{S}_{\xi}(u,v,t)$

For the third group of functions $\widetilde{f}_{\xi l}(v,t)$, the corresponding mathematical expressions of the blending surface can be taken to be

$$\widetilde{S}_{\xi}(u,v,t)=\sum_{l}\widetilde{H}_{\xi l}(u)\,\widetilde{f}_{\xi l}(v,t) \qquad (\xi=x,y,z) \tag{C1}$$

The partial differential equations (10) corresponding to the mathematical expressions $\widetilde{S}_{\xi}(u,v,t)$ are

$$(\gamma\frac{\partial^6}{\partial u^6}+\eta\frac{\partial^6}{\partial u^4\partial v^2}+\lambda\frac{\partial^6}{\partial u^2\partial v^4}+\rho\frac{\partial^6}{\partial v^6})\widetilde{S}_{\xi}(u,v,t)=0 \tag{C2}$$

The blending boundary constraints (9) corresponding to the mathematical expressions $\widetilde{S}_{\xi}(u,v,t)$ are

$$\begin{aligned}
u=0 \quad & \widetilde{S}_{\xi}(u,v,t)=\sum_{l}\widetilde{a}_{\xi l,1}\widetilde{f}_{\xi l}(v,t) && \partial\widetilde{S}_{\xi}(u,v,t)\big/\partial u=\sum_{l}\widetilde{a}_{\xi l,2}\widetilde{f}_{\xi l}(v,t)\\
& \partial^2\widetilde{S}_{\xi}(u,v,t)\big/\partial u^2=\sum_{l}\widetilde{a}_{\xi l,3}\widetilde{f}_{\xi l}(v,t)\\
u=1 \quad & \widetilde{S}_{\xi}(u,v,t)=\sum_{l}\widetilde{a}_{\xi l,4}\widetilde{f}_{\xi l}(v,t) && \partial\widetilde{S}_{\xi}(u,v,t)\big/\partial u=\sum_{l}\widetilde{a}_{\xi l,5}\widetilde{f}_{\xi l}(v,t)\\
& \partial^2\widetilde{S}_{\xi}(u,v,t)\big/\partial u^2=\sum_{l}\widetilde{a}_{\xi l,6}\widetilde{f}_{\xi l}(v,t)
\end{aligned} \tag{C3}$$

Substituting Eq. (C1) into the partial differential equation (C2), and considering the boundary constraints (C3), we obtain

$$\gamma \frac{d^6 \tilde{H}_{\xi l}(u)}{du^6} \tilde{f}_{\xi l}(v,t) + \eta \frac{d^4 \tilde{H}_{\xi l}(u)}{du^4} \frac{d^2 \tilde{f}_{\xi l}(v,t)}{dv^2} + \lambda \frac{d^2 \tilde{H}_{\xi l}(u)}{du^2} \frac{d^4 \tilde{f}_{\xi l}(v,t)}{dv^4}$$
$$+ \rho \tilde{H}_{\xi l}(u) \frac{d^6 \tilde{f}_{\xi l}(v,t)}{dv^6} = 0 \qquad \text{(C4)}$$
$$(l = 1,2,\cdots)$$

subjected to the following boundary constraints

$$\begin{array}{lllll} u = 0 & \tilde{H}_{\xi l}(u) = \tilde{a}_{\xi l,1} & \partial \tilde{H}_{\xi l}(u) / \partial u = \tilde{a}_{\xi l,2} & \partial^2 \tilde{H}_{\xi l}(u) / \partial u^2 = \tilde{a}_{\xi l,3} \\ u = 1 & \tilde{H}_{\xi l}(u) = \tilde{a}_{\xi l,4} & \partial \tilde{H}_{\xi l}(u) / \partial u = \tilde{a}_{\xi l,5} & \partial^2 \tilde{H}_{\xi l}(u) / \partial u^2 = \tilde{a}_{\xi l,6} \end{array} \qquad \text{(C5)}$$
$$(\xi = x, y, z; l = 1,2,\cdots)$$

Since the boundary functions $\tilde{f}_{\xi l}(v,t)$ $(l = 1,2,\cdots)$ are known, Eq. (C4) is a sixth-order ordinary differential equation for each of $l = 1,2,\cdots$. In order to solve Eq. (C4) subjected to the corresponding boundary constraints (C5), we first construct a trial function $\tilde{H}_{\xi l}(u)$ and make it meet the boundary constraints (C5) exactly. Then, we introduce the trial function into Eq. (C1) to obtain $\tilde{S}_{\xi}(u,v,t)$, substitute $\tilde{S}_{\xi}(u,v,t)$ into Eq. (C4), and minimize the error of Eq. (C4) to obtain the required solution.

Since Eq. (C5) involves six boundary constraints, the trial function $\tilde{H}_{\xi l}(u)$ can be taken to be a polynomial function of degree 5 plus a sine series, i. e.,

$$\tilde{H}_{\xi l}(u) = \sum_{n=0}^{5} \tilde{b}_{\xi l,n} u^n + \sum_{m=1}^{M} \tilde{c}_{\xi l,m} \sin(m\pi u) \qquad (\xi = x, y, z; l = 1,2,\cdots) \qquad \text{(C6)}$$

where $\tilde{b}_{\xi l,n}$ and $\tilde{c}_{\xi l,m}$ are unknown constants to de determined by the boundary constraints (C5) and the sixth-order ordinary differential equations (C4).

Substituting Eq. (C6) into the boundary constraints (C5), solving for $\tilde{b}_{\xi l,n}$, and inserting the obtained $\tilde{b}_{\xi l,n}$ back into Eq. (C6), the following function is obtained

$$\widetilde{H}_{\xi l}(u)=\sum_{n=1}^{6}\widetilde{a}_{\xi l,n}g_n(u)-\sum_{m=1}^{M}\widetilde{c}_{\xi l,m}\left[m\pi f_m(u)-\sin m\pi u\right] \tag{C7}$$

where $g_n(u)$ $(n=1,2,\cdots,6)$ is determined by Eq. (A8), and $f_m(u)=g_2(u)+(-1)^m g_5(u)$ $(m=1,2,\cdots,M)$.

Substituting Eq. (C7) into Eq. (C1), then introducing Eq. (C1) into Eq. (C4), and formulating the squared error of Eq. (C4) below

$$E_{\xi l}=\left[\varphi_{\xi l}(u,v)-\sum_{m=1}^{M}\widetilde{c}_{\xi l,m}\alpha_{\xi l,m}(u,v)\right]^2 \qquad (\xi=x,y,z;l=1,2,\cdots) \tag{C8}$$

with

$$\begin{aligned}\varphi_{\xi l}(u,v)=\sum_{n=1}^{6}\widetilde{a}_{\xi l,n}\Big[&\gamma g_n^{(6)}(u)\,\widetilde{f}_{\xi l}(v,t)+\eta g_n^{(4)}(u)\,\widetilde{f}_{\xi l}^{(2)}(v,t)+\lambda g_n^{(2)}\\&(u)\,\widetilde{f}_{\xi l}^{(4)}(v,t)+\rho g_n(u)\,\widetilde{f}_{\xi l}^{(6)}(v,t)\Big]\end{aligned} \tag{C9}$$

and

$$\begin{aligned}\alpha_{\xi l,m}(u,v)=&\gamma m^6\pi^6\widetilde{f}_{\xi l}(v,t)\sin(m\pi u)+\eta\left[m\pi f_m^{(4)}(u)-m^4\pi^4\sin(m\pi u)\right]\widetilde{f}_{\xi l}^{(2)}(v,t)\\&+\lambda\left[m\pi f_m^{(2)}(u)+m^2\pi^2\sin(m\pi u)\right]\widetilde{f}_{\xi l}^{(4)}(v,t)+\rho\left[m\pi f_m^{(0)}(u)-\sin(m\pi u)\right]\widetilde{f}_{\xi l}^{(6)}(v,t)\end{aligned} \tag{C10}$$

where $g_l^{(k)}(u)=d^k g_l(u)/du^k$, $\widetilde{f}_{\xi l}^{(k)}(v,t)=d^k\widetilde{f}_{\xi l}(v,t)/dv^k$, $f_m^{(r)}(u)=d^r f_m(u)/du^r$, and $f_m^{(0)}(u)=f_m(u)$, $(l=1,2,\cdots;\quad k=2,4,6;\ m=1,2,\cdots M;\quad r=0,2,4)$.

The above error $E_{\xi l}$ is a vector-valued continuous function. In order to quantify the error function, we uniformly allocate $(I+1)\times(J+1)$ sample points in the solution region $\{0\le u\le 1, 0\le v\le 1\}$ which gives $\Delta u=1/I$, $\Delta v=1/J$, $u_i=i\Delta u=i/I$, and $v_i=j\Delta v=j/J$. The squared error sum of the error function $E_{\xi l}$ at these sample points can be formulated as

$$\overline{E}_{\xi l}=\sum_{i=0}^{I}\sum_{j=0}^{J}\left[\varphi_{\xi l}(u_i,v_j)-\sum_{m=1}^{M}\widetilde{c}_{\xi l,m}\alpha_{\xi l,m}(u_i,v_j)\right]^2 \qquad (\xi=x,y,z;l=1,2,\cdots) \qquad \text{(C11)}$$

With the least squared method, we calculate $\partial\overline{E}_{\xi l}/\partial\widetilde{c}_{\xi l,m}=0 \quad (l=1,2,\cdots;\ m=1,2,3,4,\cdots,M)$ which changes Eq. (C11) into the following equation

$$\sum_{m=1}^{M}\sum_{i=0}^{I}\sum_{j=0}^{J}\widetilde{c}_{\xi l,m}\alpha_{\xi l,m}(u_i,v_j)\alpha_{\xi l,q}(u_i,v_j)=\sum_{i=0}^{I}\sum_{j=0}^{J}\varphi_{\xi l}(u_i,v_j)\alpha_{\xi l,q}(u_i,v_j) \qquad \text{(C12)}$$
$$(q=1,2,3,4,\cdots,M)$$

There are M linear algebra equations in (C12) which can be used to determine the M unknown constants $\widetilde{c}_{\xi l,m} \quad (m=1,2,3,4,\cdots,M)$.

Repeating the solution process for $l=1,2,\cdots$, all the unknown constants $\widetilde{c}_{\xi l,m} \quad (l=1,2,\cdots;m=1,2,\cdots,M)$ are obtained. Substituting them back into Eq. (C7), and introducing Eq. (C7) into Eq. (C1), the mathematical expressions are obtained as

$$\widetilde{S}_{\xi}(u,v,t)=\sum_{l}\sum_{n=1}^{6}\widetilde{a}_{\xi l,n}g_n(u)-\sum_{m=1}^{M}\widetilde{c}_{\xi l,m}\left[m\pi f_m(u)-\sin m\pi u\right]\widetilde{f}_{\xi l}(v,t) \qquad \text{(C13)}$$
$$(\xi=x,y,z;l=1,2,\cdots)$$

Figure Captions List

Fig. 1 Primary surfaces in cyan and brown at $t = 0$, 0.2, 0.4, 0.6, 0.8, and 1

Fig. 2 Blending surfaces generated by three different M values and the closed form solution (CFS)

Fig. 3 Blending surfaces at different time instants

Fig. 4 Comparison between C^1 and C^2 continuous surface blending approaches

Fig. 5 Effects of second partial derivatives

Fig. 6 Blending surfaces with $\gamma = \eta = \lambda = \rho = 1$ at different time instants

Fig. 7 Effect of the shape control parameter γ on the blending surface with $\eta = \lambda = \rho = 1$ and $t = 0$

Fig. 8 Effect of the shape control parameter η on the blending surface with $\gamma = \lambda = \rho = 1$ and $t = 0$

Fig. 9 Effect of the shape control parameter λ on the blending surface with $\gamma = \eta = \rho = 1$ and $t = 0$

Fig. 10 Effect of the shape control parameter ρ on the blending surface with $\gamma = \eta = \lambda = 1$ and $t = 0$

Fig. 11 Surface blending between linearly varying primary surfaces

Fig. 12 Surface blending between non-linearly varying primary surfaces

Fig. 13 Blending between a cubic NURBS surface and a quartic NURBS

surface

Fig. 14 Surface blending between intersecting planes with inclined trimlines

Fig. 15 Surface blending between intersecting cylinders

Fig. 16 Surface blending between a cylinder and a plane for a transmission yoke - drive shaft

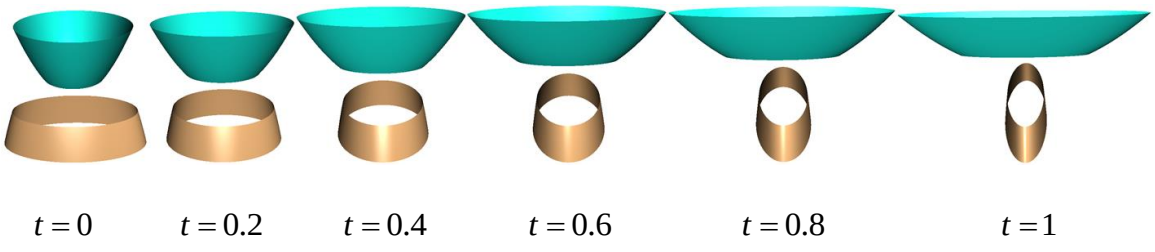

Fig. 1 Primary surfaces in cyan and brown at $t = 0$, 0.2, 0.4, 0.6, 0.8, and 1

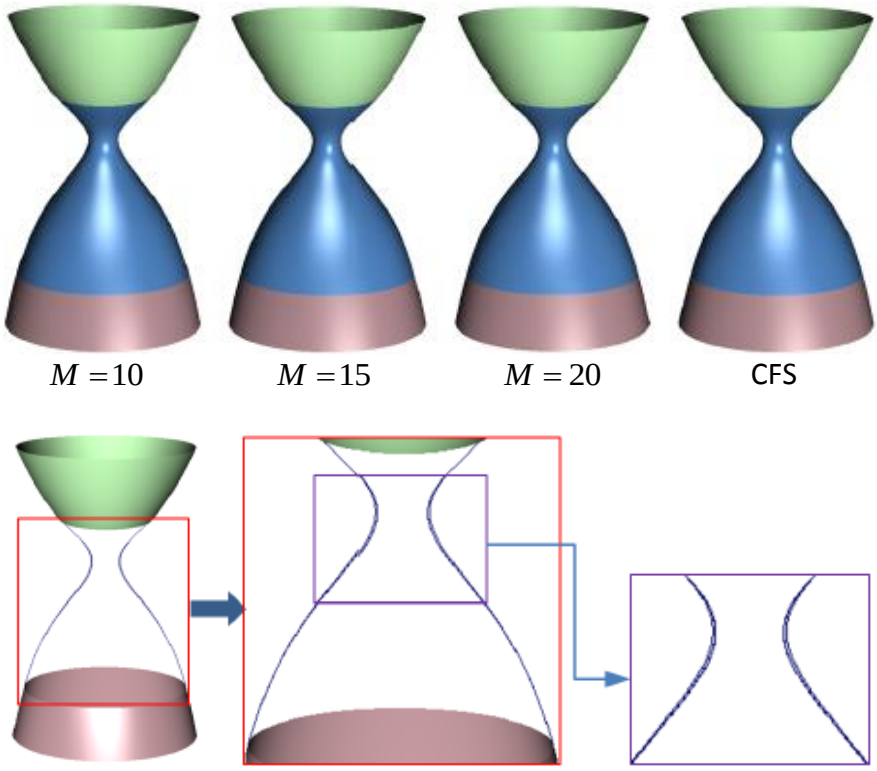

Fig. 2 Blending surfaces generated by three different M values and the closed form solution (CFS)

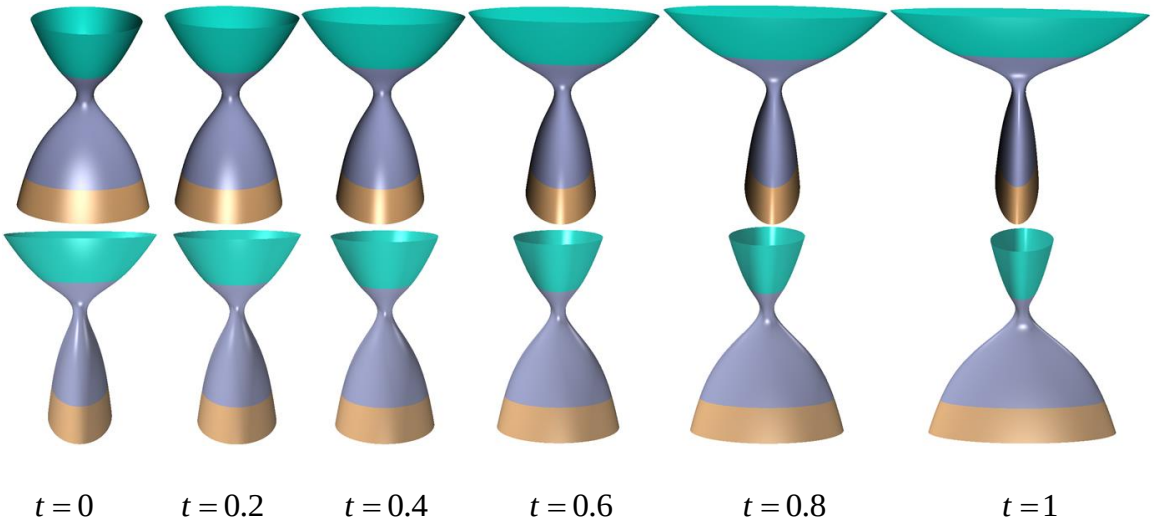

Fig. 3 Blending surfaces at different time instants

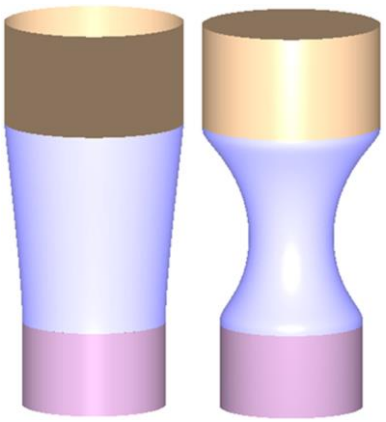

(a) (b)

Fig. 4 Comparison between C^1 and C^2 continuous surface blending approaches

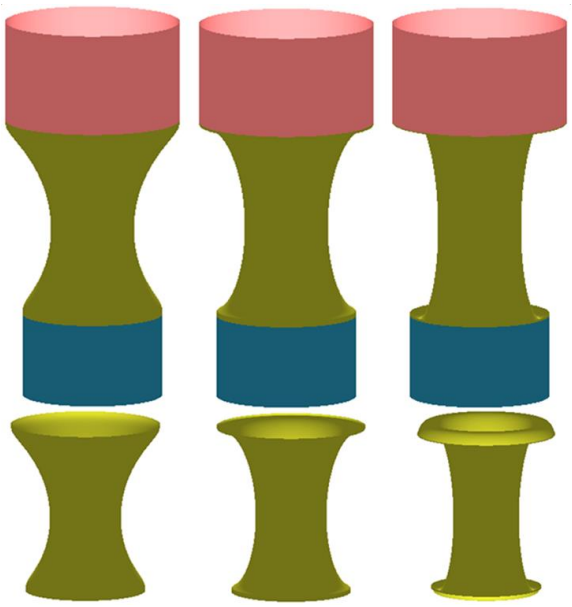

(a) (b) (c)

Fig. 5 Effects of second partial derivatives

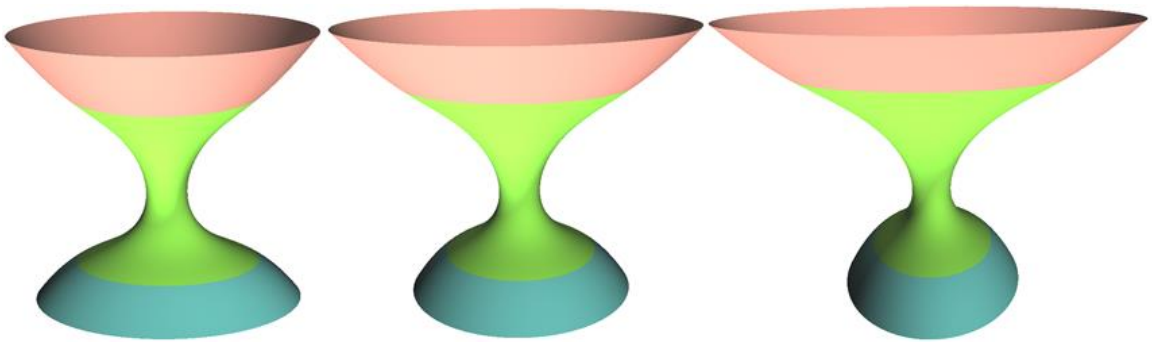

$t = 0.2$ $t = 0.4$ $t = 0.6$

Fig. 6 Blending surfaces with $\gamma = \eta = \lambda = \rho = 1$ at different time instants

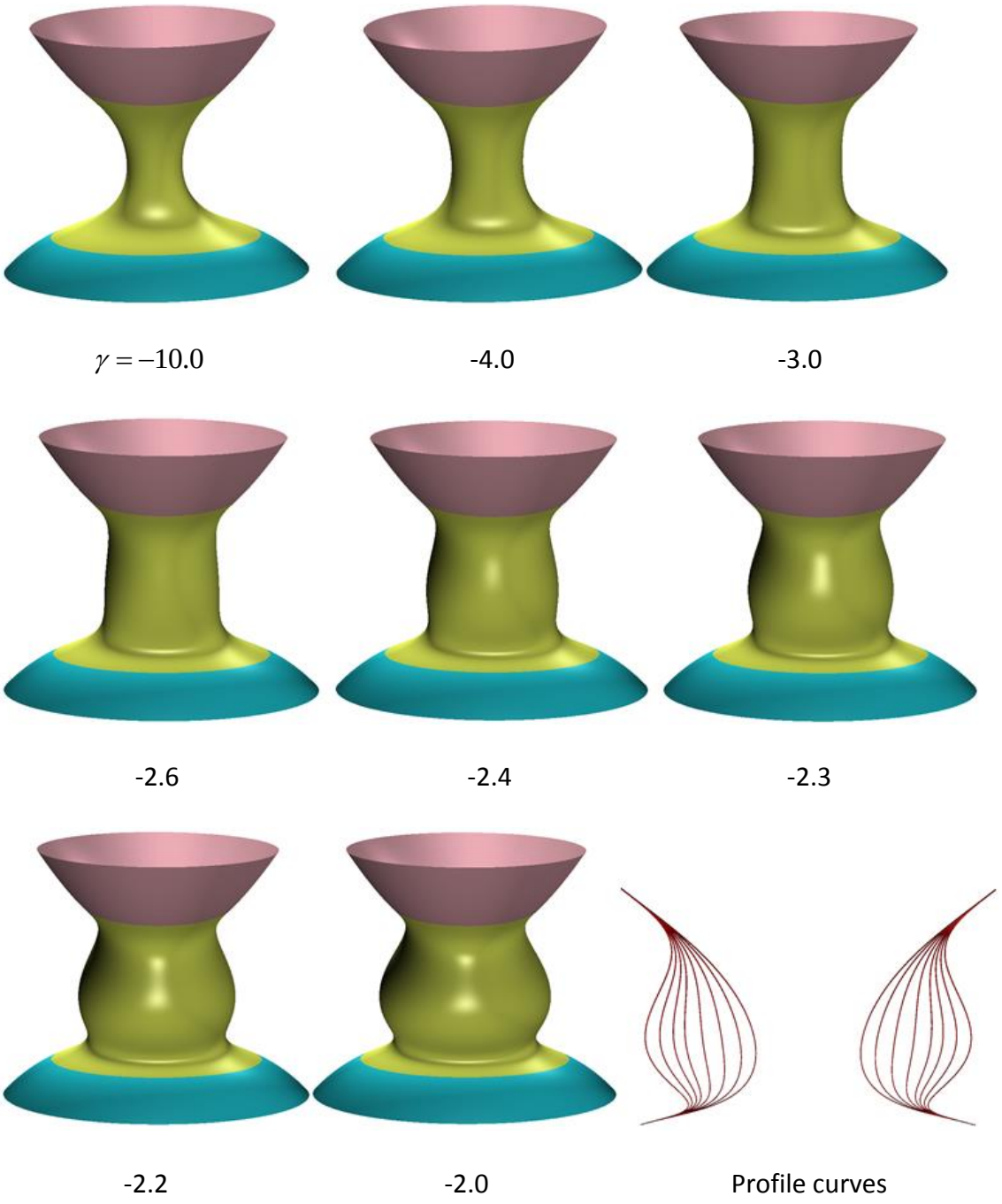

Fig. 7 Effect of the shape control parameter γ on the blending surface with $\eta = \lambda = \rho = 1$ and $t = 0$

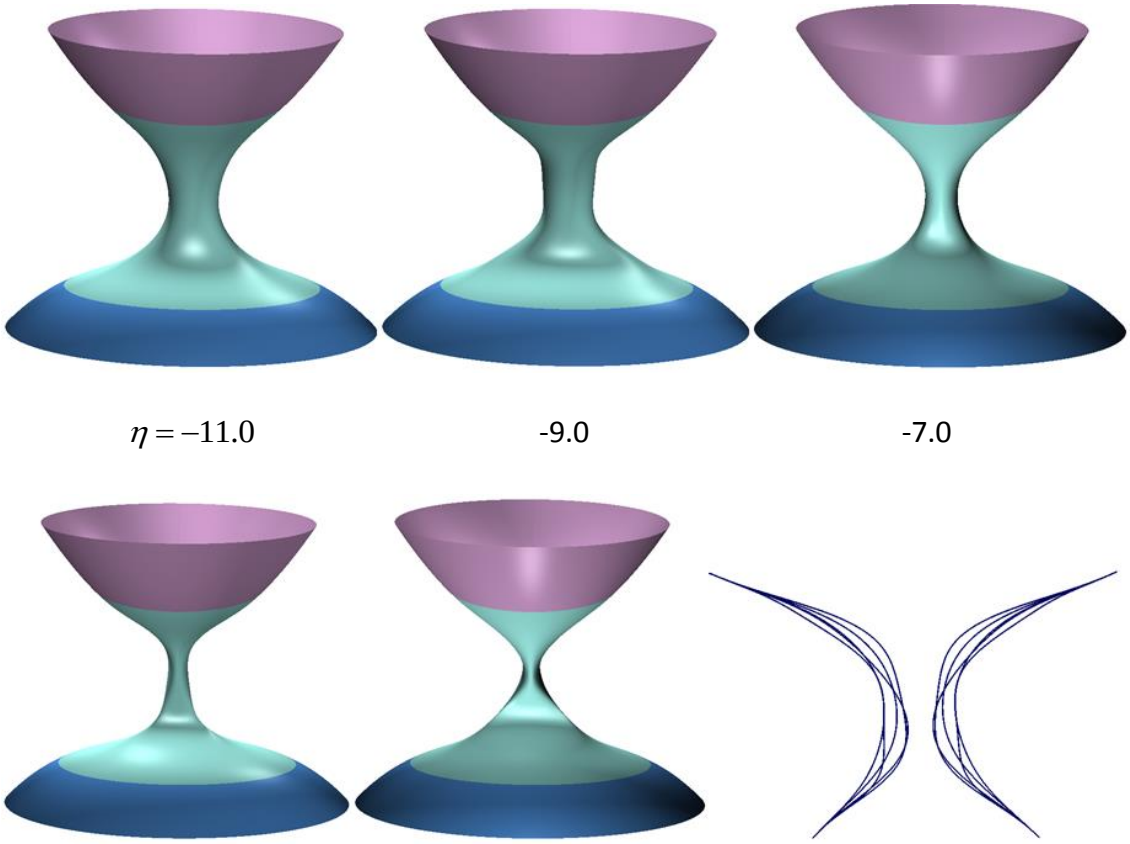

Fig. 8 Effect of the shape control parameter η on the blending surface with $\gamma = \lambda = \rho = 1$ and $t = 0$

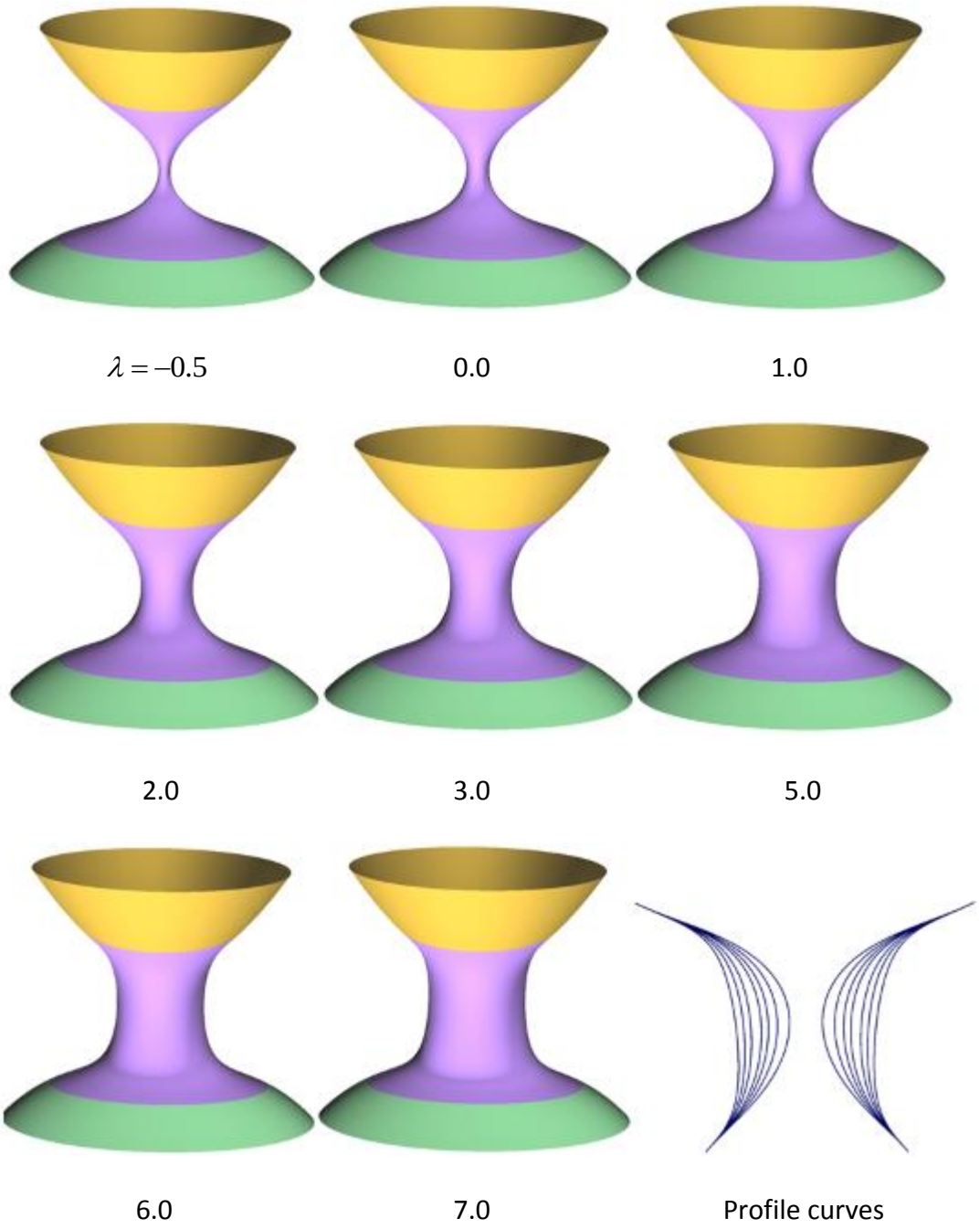

Fig. 9 Effect of the shape control parameter λ on the blending surface with $\gamma = \eta = \rho = 1$ and $t = 0$

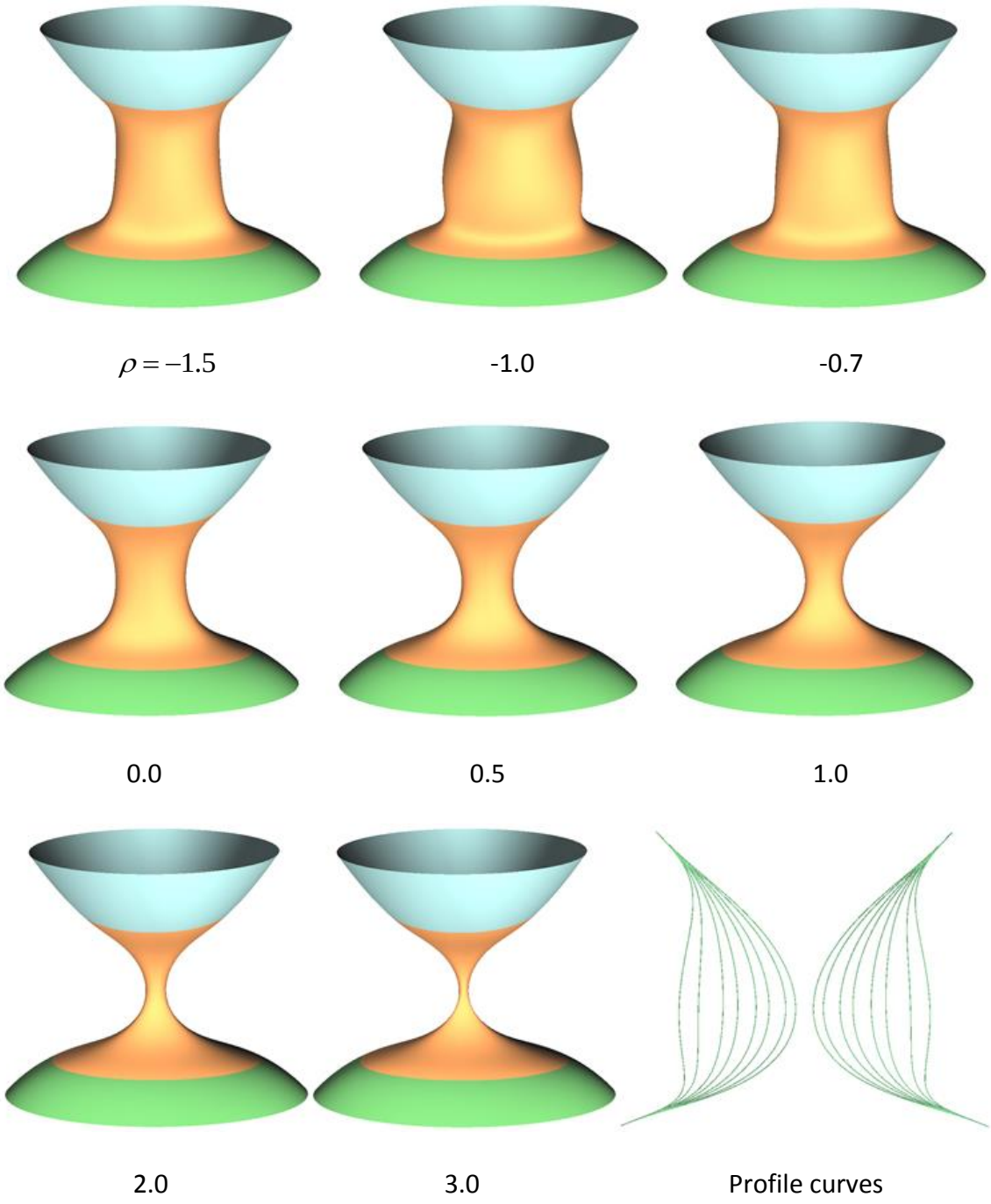

Fig. 10 Effect of the shape control parameter ρ on the blending surface with $\gamma = \eta = \lambda = 1$ and $t = 0$

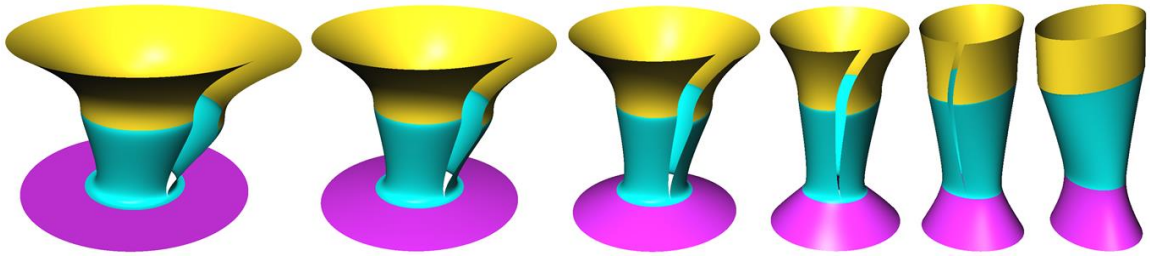

Fig. 11 Surface blending between linearly varying primary surfaces

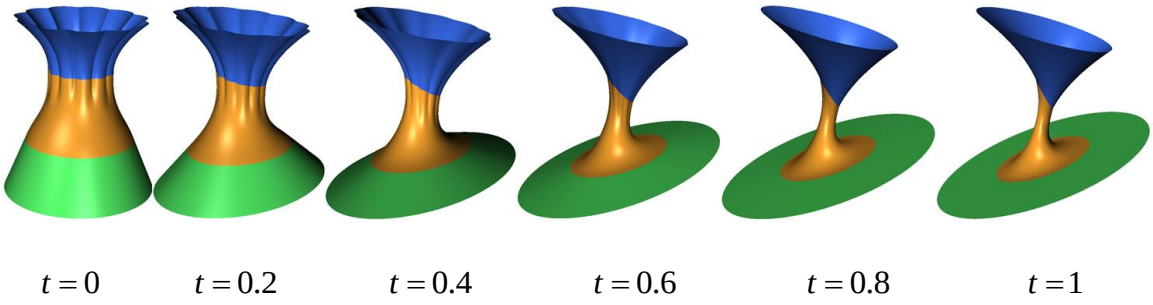

Fig. 12 Surface blending between non-linearly varying primary surfaces

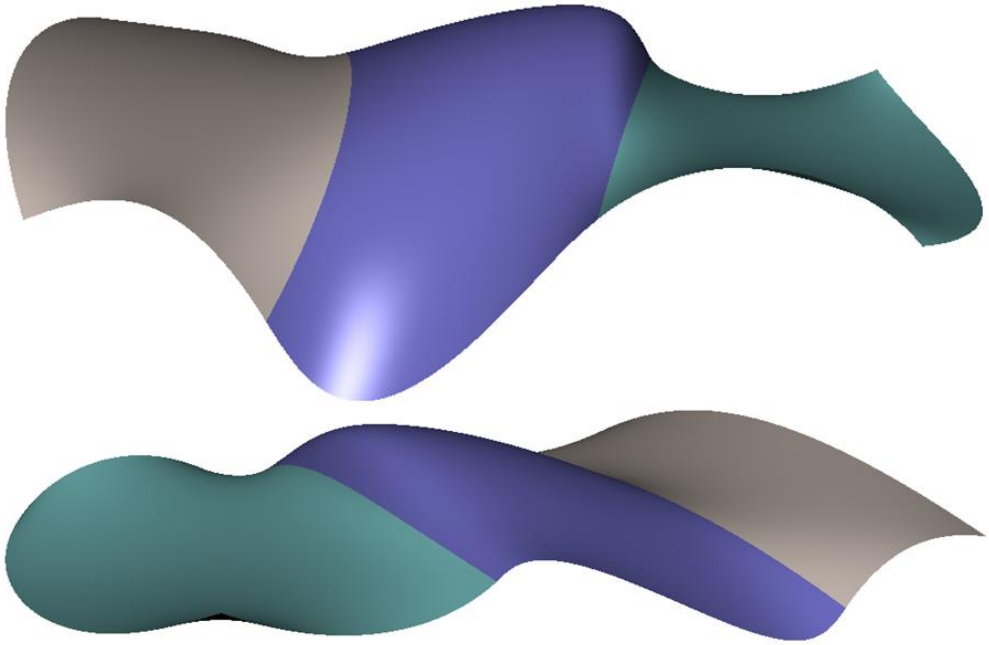

Fig. 13 Blending between a cubic NURBS surface and a quartic NURBS surface

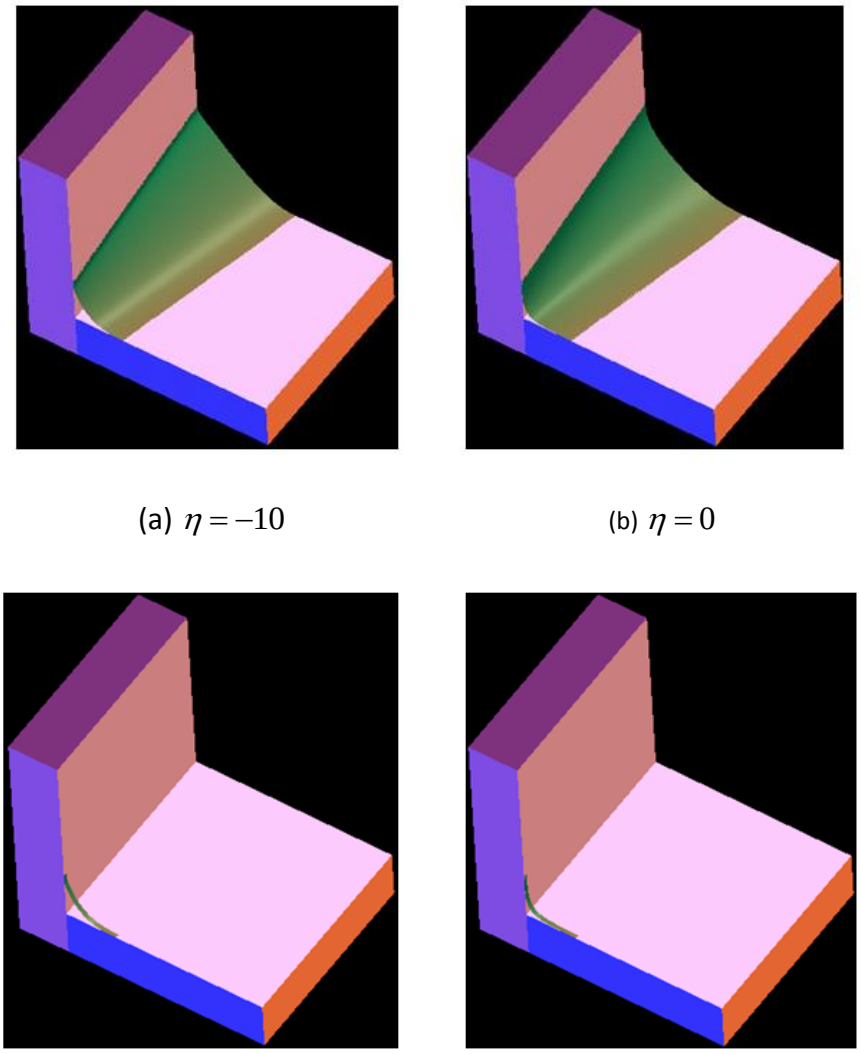

(a) $\eta = -10$ (b) $\eta = 0$

(c) $\eta = -10$ (d) $\eta = 0$

Fig. 14 Surface blending between intersecting planes with inclined trimlines

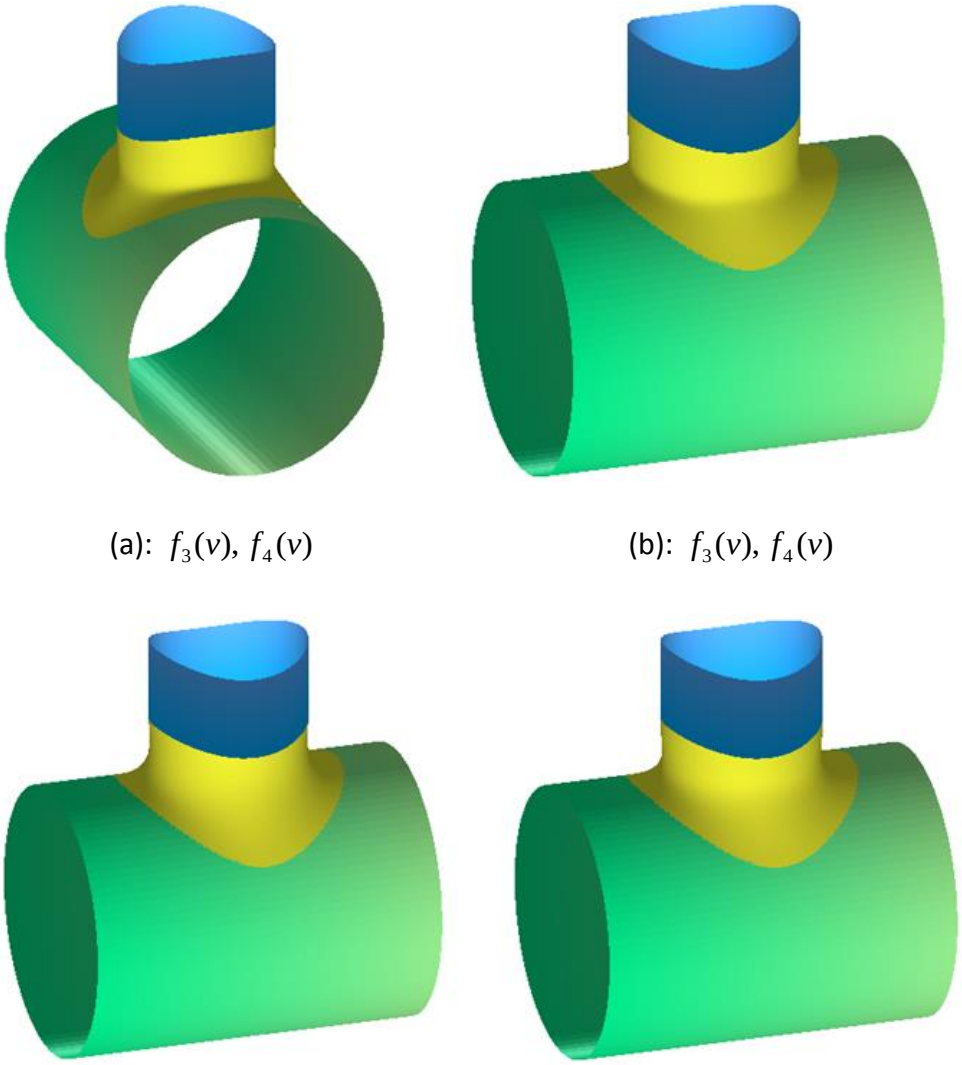

(a): $f_3(v)$, $f_4(v)$ (b): $f_3(v)$, $f_4(v)$

(c): $0.01 f_3(v)$, $f_4(v)$ (d): $f_3(v), 10 f_4(v)$

Fig. 15 Surface blending between intersecting cylinders

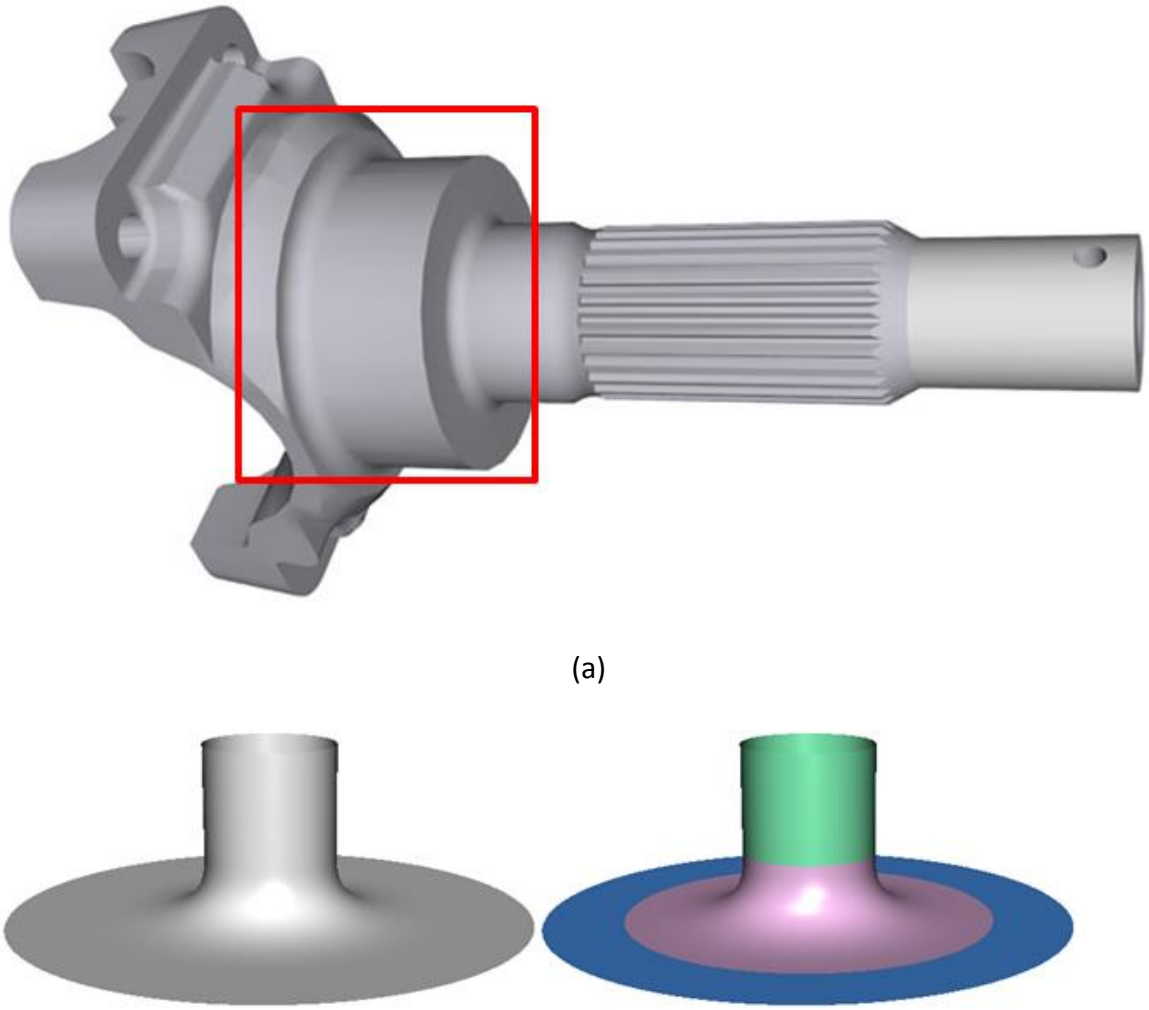

(a)

(b) (c)

Fig. 16 Surface blending between a cylinder and a plane for a transmission yoke - drive shaft

Table Caption List

Table 1 Accuracy and of the proposed approach efficiency

Table 1 Accuracy and efficiency of the proposed approach

M	10	15	20	CFS
E_1	4.35×10^{-2}	3.17×10^{-3}	2.22×10^{-5}	0
E_2	1.82×10^{-2}	1.31×10^{-3}	1.10×10^{-5}	0
E_3	1.11×10^{-2}	8.06×10^{-4}	5.64×10^{-6}	0
E_4	4.63×10^{-3}	3.34×10^{-4}	2.80×10^{-6}	0
T(ms) (51×51)	35	60	98	47
T(ms) (101×101)	69	112	197	109
T(ms) (151×151)	118	184	288	187
T(ms) (201×201)	183	269	394	339